J. Fluid Mech. (1984), *vol.* 139, *pp.* 29–65
Printed in Great Britain

The mixing layer: deterministic models of a turbulent flow. Part 1. Introduction and the two-dimensional flow

By G. M. CORCOS AND F. S. SHERMAN
University of California, Berkeley, CA 94720

(Received 22 December 1982 and in revised form 9 August 1983)

The prevalence in a turbulent mixing layer of dynamical events with a coherent history over substantial times suggests that it is profitable to study in detail entirely deterministic versions of this flow and to attempt to use a simplified synthesis of these solutions as the fundamental representation in a stochastic treatment of the layer. It is proposed that the deterministic representation of the flow be achieved by the embedding of a short hierarchy of motions which are studied in detail, though not exhaustively, in Parts 1, 2 and 3. Part 1 deals with the fundamental or first-order motion, which is the evolution of a layer constrained to be purely two-dimensional.

1. Introduction

It is often said that, since turbulent flows are unsteady solutions of the Navier–Stokes equations with random features, one has to choose one of two difficult courses to study them: the first is to solve the time-dependent equations and to average the solutions; the second is to average the equations first. It may be remarked that both courses lead to indeterminacy. The indeterminacy inherent in the second course is well known as the closure problem. That which stems from the first follows from the apparent lack of uniqueness of the solutions: if any two realizations in time, with apparently identical initial and boundary conditions, are distinctly different, averaging requires not only finding all such realizations but also assigning a probability to each. Thus it would seem that the methods of stochastic theory need be used in either case.

We suggest that the real question is: how far along the way should these stochastic tools be used? To answer it, we need to know to what extent realizations are similar to each other, or again how extensive is the space of functions that they occupy. In yet other words, we need to explore whether one can construct a sufficiently recognizable portrait of a given turbulent flow or if the flow has, so to speak, so many faces that a single portrait would convey no useful recognition. What we mean by a portrait is a prototype of the flow, made up of very few plausible and tractable time-dependent solutions of the Navier–Stokes equations.

The massive attention recently paid to what is called organized or coherent structures can be interpreted in this light. For instance, the striking shadowgraphs obtained at high Reynolds numbers by Brown, Roshko, and their associates (e.g. Roshko 1976) are direct evidence that, while a turbulent shear layer has a number of stochastic features and may appear disorderly (especially when observations are made in time at one point), an individual panoramic realization displays an intriguing measure of complex order. Also, different realizations, while not identical, have a very

strong family resemblance. Such observations suggest that dynamical laws operate almost deterministically over very substantial times. This provides a strong incentive for first studying deterministic models of turbulent flows. A stochastic treatment can be used later to account for the necessarily random occurrence of initial perturbations and perhaps also to approximate those dynamical details for which we may fail to provide a deterministic description.

This approach attracts us because, as we shall show, rather complex features of a real shear flow (the shear layer) resemble strongly a suitably simplified and entirely deterministic version of this flow.

Fluid-mechanical paradigms have been used in the study of turbulence for a number of years. For instance, Synge & Lin (1943) constructed a homogeneous isotropic flow by randomly superposing Hill spherical vortices, and inferred, among other things, a law for the decay of the two-point correlation function for large separation distances. Townsend (1951) attempted to gain an idea of the fine details of turbulence by studying simple models for the straining of vortex sheets and tubes. Corrsin (1962) and Tennekes (1968) pursued the same idea, though somewhat less specifically to discuss the intermittency of the small scales and its effect on the kurtosis of the probability density of velocity derivatives. Saffman (1968) explored the consequences of averaging a two-level hierarchy of motions of random orientation, following a motivation that is very similar to ours.

But in the past the paradigms were selected from the general store of special solutions of the equations of motion without enquiring in detail about the plausibility of their presence in the course of the dynamical history of the flow. Such an inquiry generally taxes excessively the means of unaided classical analysis. Thus the straining field which concentrates vorticity and steepens local gradients could only be surmised but not described. By now a growing body of knowledge concerning the nature of large-scale strain is becoming available, primarily from numerically solved initial-value problems. This specific knowledge should allow one to study the birth and growth of a hierarchy of secondary motions which depend on or are grafted onto specific so-called large-scale structures.

We suspect that a hierarchy of motions can be traced only if it is made of very few fundamentally different types of motions, a property that needs to be demonstrated. We also assume that one elementary motion can serve as the base flow for the next, which is to say that the interaction between the two is primarily unidirectional rather than strongly reciprocal. This assumption cannot be granted *a priori* either, but it is not necessarily vitiated by the nonlinearity of the Navier–Stokes equations. For instance, it is the basis of boundary-layer theory, the boundary layer being grafted onto a potential flow which it affects only slightly. For hierarchies of interest, as for boundary layers, verification of this assumption can be made *a posteriori*.

To return to our problem, we note, and will illustrate later, a basic difference between the traditional eddy of what we might call the ritual language of turbulence theory and the elementary motions that we have in mind: it is that the constitutive elements of a stochastic theory of turbulence are chosen for their mathematical properties (they are usually generalized Fourier transforms of the realizations) and not because they resemble even vaguely a possible flow. It is typical of such elements that each one has one space scale, for instance, that an infinite number of them is required to represent the flow, and that one needs to consider the interaction between them all. Assumptions required to simplify this interaction are thus made on representations that have no physical counterparts, a great hindrance to one's

physical intuition or sense of analogy. On the other hand, our eddies, i.e. our elementary-flow candidates, are particular solutions of almost-singular partial differential equations, and so each one has in general more than one space scale, like almost all non-trivial solutions of the Navier–Stokes equations in unbounded space. For the same reason, each one embodies an understandable dynamical evolution.

The fact that each solution is characterized by several very different lengthscales causes difficulty in relating the language of a dynamical model to the usual language of turbulence as a random field. For instance, while a particular solution may be termed an eddy with a defined kinetic energy, that energy cannot be assigned to a single lengthscale or to a narrow range of scales. As a result, the classical description of energy flow through wavenumber space (the cascade) does not have any clear correspondence with the interaction between dynamical eddies of this type. That interaction appears in a dynamical model as the result of the instability of a special solution. The instability generates new motions, some with larger scales, some with smaller ones. As a result the range of possible lengthscales of motion increases, but (and this is one of the attractive features of the approach) the number of different types of dynamical structures, which together can generate the whole range of lengthscales usually associated with turbulence, is small.

We shall see for instance that the sequential two-dimensional instability of the original laminar shear layer together with the three-dimensional instability of the resulting spanwise vorticity distribution yields motions in which one readily identifies, aside from a lingering scale related to the layer initial thickness, an overall widthscale which grows linearly on the average, an intermediate, Reynolds-number-dependent scale for vorticity cores and a prominent Taylor microscale. We have not yet found an unambiguous dynamical path to scales smaller than the Taylor microscale.

The approach that we suggest and for which a start is made below in the specific case of a free shear layer offers in general two interesting areas of study to the fluid-dynamicist.

The first is the determination of the evolution of an initial distribution of vorticity, given certain constraints which prevent the unwanted generation of excessive details. Such constraints can be restriction to a two-dimensional or axially symmetric motion, to a low Reynolds number, or to periodicity in space. Whereas viscosity is often of minor importance in the evolution of the large-scale basic motion, the inviscid equations may lead to artificial complications requiring additional filters (see Zabusky & Overman 1981). Contemporary accounts of such problems include Amsden & Harlow (1964), Zabusky & Deem (1971), Christiansen (1973), Chorin (1973, 1978), Acton (1976), Patnaik, Sherman & Corcos (1976), Guiraud & Zeytounian (1977, 1979), Chorin *et al.* (1978), Ashhurst (1979), Zabusky, Hughes & Roberts (1979), Leonard (1980), Riley & Metcalf (1980), Zabusky (1981) and Overman & Zabusky (1981).

The reliability of this type of calculation should be helped in the future by the rapid development of the mathematical foundations of numerical approximations to solutions of the Navier–Stokes and Euler equations, in particular by means of vortex elements (Moore 1976; Hald 1979; Beale & Majda 1981, 1982).

But so far many important geometries, i.e. many initial vorticity distributions, have received scant attention. Some interesting developments of a somewhat different type, but clearly aimed in the same direction, are reported by Cantwell (1981).

The second area is, of course, the study of the secondary flows which these motions can create.

In what follows, we discuss both the primary flow and flows that derive from it

in the special case of the free shear layer. We propose a hierarchy of motions which is made of three tiers. The first tier or first-order motion is discussed in the remainder of this first article. It is defined as that which results from the layer's two-dimensional instability. We use numerical solutions to discuss its nature and some of the more important properties of this restricted unstationary flow. They include details of roll-up and pairing and of the history of strain during these events. We also examine to what extent and how, according to the two-dimensional model, the initially non-homogeneous distribution of a transported diffusive scalar is homogenized by the combination of differential advection and molecular diffusion.

These characteristics of the two-dimensional flow in turn govern the development of additional degrees of freedom: In Part 2 of this study (Corcos & Lin 1984), starting with a simple shear layer slightly perturbed by both two-dimensional and three-dimensional disturbances, we repeat our nonlinear calculations of the growth of the two-dimensional motion and simultaneously use this flow as the time-dependent parent flow upon which the (linearized) three-dimensional perturbations grow. This leads to the development of second-order motion. The calculation demonstrates that the dynamical effect of the new motion on the first-order flow is not considerable. It reveals that the layer becomes segregated into regions in which the kinetic energy of the secondary flow is quite weak (though the value of the streamwise vorticity may reach a maximum) and regions of intense magnitude and production rate of three-dimensional kinetic energy. It also shows that pairing can inhibit the continuous growth of this motion.

In Part 3 (Lin & Corcos 1984) we use idealizations of the parent flow to study first simple analytical linear models of the second-order flow and then numerical solutions† of the corresponding nonlinear evolution of this flow. The nonlinear study shows that the distribution in space of streamwise vorticity becomes radically different when its circulation is strong enough. The rate of molecular mixing of scalars is also strongly dependent on this distribution, i.e. on the type of balance which is possible between strain (from the first-order flow), self-induction, and diffusion of streamwise vorticity.

Finally, we follow the birth and development of one possible third-order motion by using as a base an idealized second-order flow. The former is made of smaller eddies which grow out of the instability of the latter if the initial Reynolds number is sufficiently large. We encounter roll-up and limited pairing of streamwise vorticity, but the outcome is deeply affected by the streamwise strain. In fact, the flow evolution here, and the one mentioned above, lead through very different dynamic histories, essentially to the same end result.

The reader will become aware that the proposed portrait of the shear layer is far from completed. It would be more accurate to characterize the following as a series of photographs, too anatomically detailed to be directly incorporated into a functional model, together with a series of preliminary sketches. Nevertheless, it is hoped that the approach will be viewed as fruitful enough to pursue in this as well as in other contexts.

2. The shear layer

2.1. *Motivation*

The shear layer is a turbulent zone of transition between two parallel streams (1 and 2) each with a uniform velocity (U_1 and U_2) both assumed to be in the x-direction. It can easily be created in the laboratory and it has been the object

† See also the asymptotic analysis by Neu (1984*b*).

of numerous studies of different types. It is a particularly attractive flow for several reasons.

(1) It is a prototype of a separated flow or of counterflowing streams. It is also approximated in some combustors and chemical lasers. It is found in natural flows whenever two streams of different velocity merge as in the discharge of a river in a lake or an estuary, although, in nature, the density of the fluid is frequently stratified so that buoyancy may play an important role in the development of the layer.

(2) The vorticity is initially unidirectional and of one sign. It possesses a non-trivial invariant for all times, regardless of local production (e.g. through baroclinicity), i.e.

$$\frac{1}{L}\int_0^L \int_{-\infty}^{\infty} \Omega_2 \, dz \, dx = U_1 - U_2 = \Delta U = 2U = \text{constant},$$

where x is the streamwise, y the spanwise, and z the cross-stream direction, Ω_2 is the y-component of the vorticity $\boldsymbol{\Omega}$ and L is a suitable length.

(3) Detailed finite-difference solutions of the two-dimensional problem have been obtained (for relatively low values of the Reynolds number), from which the behaviour of the flow for all times can be inferred approximately: The initial roll-up phase of the nonlinear instability that characterizes it has been studied on at least six separate occasions by finite differences (Amsden & Harlow 1964; Tanaka 1975; Deem 1977; Patnaik, Sherman & Corcos 1976; Acton 1976; Peltier, Halle & Clark 1978; Riley & Metcalf 1980). The latter also calculated interaction with a first subharmonic. The two-dimensional problem has also been attacked by a variety of alternative numerical techniques (see e.g. Ashurst 1979; Delcourt & Brown 1979).

(4) The shear layer has in addition been studied in extraordinary detail in the laboratory at high and low Reynolds numbers (see e.g. Liepmann & Laufer 1947; Bradshaw 1966; Wygnanski & Fiedler 1970; Winant & Browand 1974; Brown & Roshko 1974; Batt 1975; Browand & Weidman 1976; Konrad 1977; Pui & Gartshore 1978; Breidenthal 1978; Koop & Browand 1979; Wygnanski *et al.* 1979; Latigo 1979; Hussain & Clark 1981; Browand & Troutt 1980).

(5) Finally, as has already been mentioned, it is perhaps in the turbulent shear layer that dynamical coherence is both most strikingly apparent and most successfully modelled.

2.2. *Time and space development*

If a shear layer originates in the merger of two streams, it will develop in the streamwise direction. This is almost always the natural way in which such flows occur. It will be convenient to call it an S-layer. On the other hand, the mathematical and the numerical study of such layers are far easier for a flow that is initially x-independent and grows in time, and so a good deal of our information originates in this version of the problem which we shall call a T-layer. When $2(U_1 - U_2)/(U_1 + U_2) \ll 1$ the two problems are easily shown to be equivalent† if a Galilean transformation involving the average velocity $\frac{1}{2}(U_1 + U_2)$ is used. Otherwise there are some qualitative differences between them, since the governing equations are parabolic in time, while they are elliptic in the streamwise coordinate. Thus an event (such as the coalescence of two vortices) which occurs in a natural flow somewhere downstream of the splitter plate induces a change in velocity everywhere in the flow, including upstream, whereas, for the layer developing in time, such an event is clearly unable to affect the previous development of the flow. In addition in the S-layer (unlike the T-layer) there are no symmetries around any spanwise axes. As a consequence, the average

† For a strictly incompressible fluid.

rate of growth of the layer into the two uniform streams need not be the same; this is of importance in problems involving reaction and combustion between the fluids from the two streams.†

These differences between strikingly similar-looking flows has to be kept in mind. It introduces a measure of uncertainty in the comparison between theory or numerical solutions and experimental observations.

2.3. *Initial conditions*

The initial conditions can also be conceived in more than one way. We shall generally take them to be a laminar shear flow with a z-wise monotonic variation in velocity between two streams upon which is superimposed a three-dimensional spectrum of infinitesimal time-dependent disturbances. Shear layers downstream of a splitter plate will start with the merger of two boundary layers which may be turbulent at the plate trailing edge. Thus the velocity profile may not be monotonic for some distance downstream of the origin, and the perturbations present in the flow may be finite. While these differences will also be kept in mind in any comparison between model and experiments, we will consider these two possible (but not unavoidable) experimental complications as outside the province of the problem.

3. The two-dimensional instability of the shear layer

3.1. *Introduction*

This instability can be described as the endless redistribution in space of the vorticity Ω_2 that the layer possesses initially. It is made up of two chronologically (or x-wise) distinct phases.

During the first phase, this redistribution occurs on the lengthscale of the initial layer thickness δ_i. In the T-layer, a concentration of vorticity appears with a periodicity in the streamwise direction x and a characteristic height in the lateral direction z, both of which are proportional to δ_i. An additional strain-induced scale $(\nu\delta_i/\Delta U)^{\frac{1}{2}}$ also arises naturally. Here ν is the kinematic viscosity. The second phase is the result of a sequential instability of the vorticity distributions to subharmonic perturbations. Each one leads to the coalescence of the previous concentration of vorticity into larger and more distant lumps. The coalescence of vortex centres two at a time is most frequent, and this leads to a binomial growth of both the circulation around each vortex and of the spacing between vortices. The time required for a pairing also doubles for each pairing so that the growth of the layer is, on the average, linear in time.

3.2. *Methods of study*

Many characteristics of the turbulent shear layer have been revealed by optical techniques or measured in laboratory experiments. The visual records (e.g. the dye films of Winant & Browand (1974), the spark-shadowgraphy for the Laplacian of the index of refraction in Brown & Roshko (1974), the visible products of reaction in Breidenthal (1978), the dye fluorescence under excitation by a sheet of laser light of Dimotakis, Miake-Lye & Papantoniou (1982)) have played a crucial role in directing attention to possible dynamical events. But of the measurements, only a fraction are directly related to the quantities most necessary to the understanding of the flow dynamics. For instance, even the spanwise component of vorticity is rarely reported

† I am indebted to J. A. Broadwell for pointing this out. The first experimental observation of a difference in entrainment rates seems to be due to Konrad (1977).

(for examples, see Browand & Weidman 1976; Hussain 1980). When it is, it most probably suffers, even with conditional sampling, from poor resolution as a result of the lack of precise repeatability of the flow pattern.

The linear theory of shear-layer stability is well developed for both kinds of shear layers. But it applies to a very early part of the layer evolution, and only if the initial layer perturbations are very small. According to both that theory and experiments, the growth rate of the most unstable perturbations is large enough (unless the Reynolds number is uncommonly low) so that the linear equation that determines the eigenvalues rapidly becomes inaccurate. Furthermore, methods based on expansions in powers of the perturbation amplitude cannot be expected to improve the accuracy of linear theory, except for discouragingly short times.

On the other hand, a number of numerical simulations of the full equations have been carried out successfully. These may be viewed as numerical experiments which are particularly well suited to yield the history of any desired dynamical variable. In the following discussion we shall make extensive use of the results of simulations by finite differences. The numerical scheme used in all these calculations is the second scheme discussed in Patnaik *et al.* (1976, henceforth called (I)). Full details are found in Sherman (1979).

3.3. *Model and notation for the two-dimensional motion*

The mathematical model for the numerical simulations is that used in (I), with the single exception that the variations in density are now assumed to yield negligible buoyancy forces. For reasons that will appear later, we nevertheless solve for the evolution of a passive scalar ρ which could represent any diffusive scalar attribute such as concentration of a dilute constituent of the fluid.

If x and z are the streamwise and cross-stream directions, p the pressure, ρ_0 the average density, ν the kinematic viscosity, ρ the passive scalar density and D the diffusivity of ρ, the equations are then

$$\frac{\partial u}{\partial t}+u\frac{\partial u}{\partial x}+w\frac{\partial u}{\partial z}+\frac{1}{\rho_0}\frac{\partial p}{\partial x}=\nu\left(\frac{\partial^2 u}{\partial x^2}+\frac{\partial^2 u}{\partial z^2}\right), \tag{3.1a}$$

$$\frac{\partial w}{\partial t}+u\frac{\partial w}{\partial x}+w\frac{\partial w}{\partial z}+\frac{1}{\rho_0}\frac{\partial p}{\partial z}=\nu\left(\frac{\partial^2 w}{\partial x^2}+\frac{\partial^2 w}{\partial z^2}\right), \tag{3.1b}$$

$$\frac{\partial \rho}{\partial t}+u\frac{\partial \rho}{\partial x}+w\frac{\partial \rho}{\partial z}=D\left(\frac{\partial^2 \rho}{\partial x^2}+\frac{\partial^2 \rho}{\partial z^2}\right), \tag{3.1c}$$

$$\frac{\partial u}{\partial x}+\frac{\partial w}{\partial z}=0. \tag{3.1d}$$

The streamwise velocity changes from $-U$ to $+U$ and the scalar from $+\frac{1}{2}\Delta\rho$ to $-\frac{1}{2}\Delta\rho$ as the layer is crossed from below to above. The flow to which perturbations are added is that which would be caused by molecular diffusion from initial coplanar discontinuities of scalar concentration and horizontal velocity at $z=0$. Thus the profiles are

$$u=U\,\mathrm{erf}\left(\frac{\pi^{\frac{1}{2}}z}{2\delta_i}\right),\quad \rho=-0.5\Delta\rho\,\mathrm{erf}\left(\frac{(\pi Pr)^{\frac{1}{2}}z}{2\delta_i}\right),$$

where $Pr=\nu/D$ = Prandtl or Schmidt number, δ_i is half the maximum slope thickness of the base flow profile at $t=0$, $\delta_i=U[(\partial u/\partial z)_{\max}]^{-1}$. We define

$$Re=\frac{U\delta_i}{\nu},\quad \Omega_2=\frac{\partial u}{\partial z}-\frac{\partial w}{\partial x}.$$

All computational results are given for a non-dimensional form of (3.1) in which the velocity scale is U, the scale for the passive scalar ρ is $\Delta\rho$, the lengthscale is the wavelength λ of the initial disturbance (when several initial disturbances are introduced, λ is the length of the shortest wave), and the timescale is λ/U. We define $\alpha = \delta_i k$, where $k = 2\pi/\lambda$.

The material interface of the flow is defined as made up for all times of the fluid particles that were initially endowed with the value $\rho = 0$ of the scalar attribute. These particles are initially found near $z = 0$ along a curve which depends on the nature and amplitude of the initial perturbations. The scalar γ is defined on the material interface as its proportional rate of extension. If u_s is the component of velocity tangent to the interface at a point, s the distance along the interfacial curve and δl a small arc of the curve at the point, then

$$\gamma = \lim_{\delta l \to 0} \frac{1}{\delta l} \frac{\mathrm{d}\delta l}{\mathrm{d}t} = \frac{\partial u_s}{\partial s}. \tag{3.2}$$

Both γ and the Lagrangian coordinates of identified points of the interface are obtained in the numerical simulation by selecting a number of points on the interface at the initial instant and displacing them at each timestep according to the velocity interpolated for the point location from the velocities obtained on the Eulerian grid.

3.4. *Two-dimensional instability, first stage: the roll-up*

This stage has its origin in the well-known so-called inviscid instability of a vorticity distribution endowed with a maximum to small perturbations periodic in the streamwise direction (see e.g. Drazin & Reid 1981).† A few features of this instability are of particular importance.

In a streamwise-developing layer, let the x component of velocity tend to U_1 as $z \to \infty$ and to $U_2 < U_1$ as $z \to -\infty$. Then the following hold.

(*a*) Unstable perturbation wavenumbers are such that $0 < k < a/\delta_i$, where a is a constant of order unity. The fastest-growing perturbation has some intermediate value of k, and its exponential growth rate is of the order of $\Delta U/2\delta_i$. But, while the perturbation amplitude is small, a continuous range of wavenumbers grow simultaneously.

(*b*) The wave velocity c_r is bounded by the extreme values of U:

$$U_2 < c_r < U_1.$$

In a coordinate system in which $U_1 > 0$, $U_2 < 0$, this leads to the necessity for u, the x-component of perturbation velocity, to vanish either at isolated points or on streamlines which are closed on themselves (Kelvin's cat's-eyes). The finite disturbances also have this property, which turns out to be of profound importance both for the nature of the large-scale instability and in that these expanding recirculating regions provide the environment required for rapid mixing.

The physical aspect of the initial instability is described by Batchelor (1967, p. 516) and by Drazin & Reid (1981) for a single long wave ($\alpha \ll 1$). It is worth noting that the perturbed vorticity distribution is strained by the velocity field associated with it in such a way that one part of the vorticity layer is foreshortened while the other is stretched.

† The linear stability problem is presented more formally in Part 2 in a three-dimensional context.

3.4.1. *Selection*

An early consequence of the increasing nonlinearity of the flow is suggested by laboratory observations: even when a continuous spectrum of small disturbances is present, a dominant wavelength seems to impose itself at least temporarily and to inhibit the growth of perturbations of neighbouring wavelengths, which are also unstable individually but which either grow less rapidly or had initially a smaller amplitude. Thorpe (1971) gives a striking photographic illustration of this phenomenon for a moderately stratified shear layer. The selection seems far sharper than the one initially imposed by linear theory so that, as the wave reaches large amplitudes, it seems possible to represent its velocity components at any given streamwise station x by

$$f(t) \sum_{n=1}^{\infty} A_n(z) \cos n\omega t,$$

where $f(t)$ is, on the scale of $2\pi/\omega$, a slowly modulating random function of time. A detailed documentation of this point must await either experiments in which selected perturbations of neighbouring frequencies are forced simultaneously on the initial layer, or an equivalent numerical study for the development of a two-dimensional layer downstream of a splitter plate.†

In any case, this observation encourages the use in numerical simulations of initial conditions which are much simpler than a continuous spectrum of perturbations. For the study of the first stage of the instability, the chosen initial perturbation is the eigenfunction of the wave that, according to linear theory, has the largest growth rate. This wavelength is very close to that which is generally observed to grow initially on a layer created from two quiet streams.

3.4.2. *The nonlinear stage*

The nonlinear development of the first stage of instability can be followed through figures 1(*a–d*) taken from a typical simulation for which $Re = 100$ and $\alpha = 0.43$. Streamlines and interfacial markers are shown on the same figures. As the interface is distorted, its length evidently increases so that it is stretched on the average. But the successive figures show that the stretching is quite uneven. Figure 2, a contour map of γ as a Lagrangian function of time and origin on the material interface, illustrates this point further and shows that the proportional rate of stretching alternates positive and negative values.

The sequence in figures 1(*a–d*) shows that the interface rolls up into a spiral, and that the markers migrate rapidly inward along the spiral and accumulate near its focus.‡ The stagnation point on both edges of the figures is a saddle for the velocity field, whose neighbourhood is systematically depleted of markers and near which the material interface is consistently stretched.

By continuity, positive values of γ imply negative strain in a direction normal to the material interface, so that near the saddles both vorticity and scalar gradient

† In the numerical formulation of the layer developing *in time*, streamwise boundary conditions are taken as periodic, and the wavelengths (rather than the frequencies) of the two competing perturbations have neighbouring values. Then the length of the first commensurate subharmonic which is the minimum grid length is excessively large. Thus the time-developing version of the numerical problem is ill-suited to the study of this type of interaction.

‡ Thus, to obtain a reasonable concentration of markers along the interface at some representative time during the roll-up, one must initially crowd them near the saddles as in figure 1(*a*).

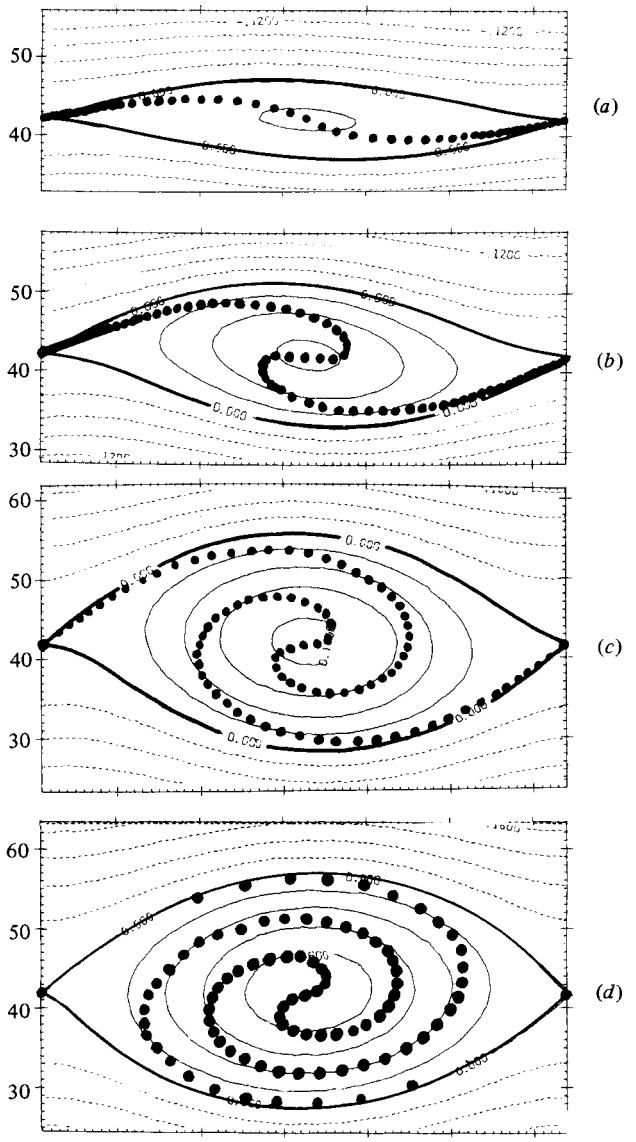

FIGURE 1. The first stage of instability: streamlines and material interface; $\alpha = 0.43$, $Re = 100$: (*a*) $\tau = 0.5$; (*b*) 1.0; (*c*) 1.5; (*d*) 2.0. The heavy line is the cat's-eye. The dots are interfacial markers.

layers which initially straddle the interface thin out in spite of lateral diffusion and form 'braids'. This effect is naturally more striking for high than for low Reynolds (or Péclet) numbers, but it is apparent in figures 3 (*a*, *b*) (vorticity) and 4 (*a*, *b*) (density or scalar concentration) for $Re = 100$ and $Pr = \nu/D = 1$.

Comparison of these figures also shows that vorticity Ω_2 and concentration ρ behave differently. The integral over the whole domain of the spanwise vorticity is an invariant as we have noted, but the integral across the layer at a given value of s is not: the local vorticity migrates away from the saddle points and towards the points of accumulation in such a way that, where γ is positive, the total shear across the layer and the local value of the vorticity both steadily decrease. On the other hand,

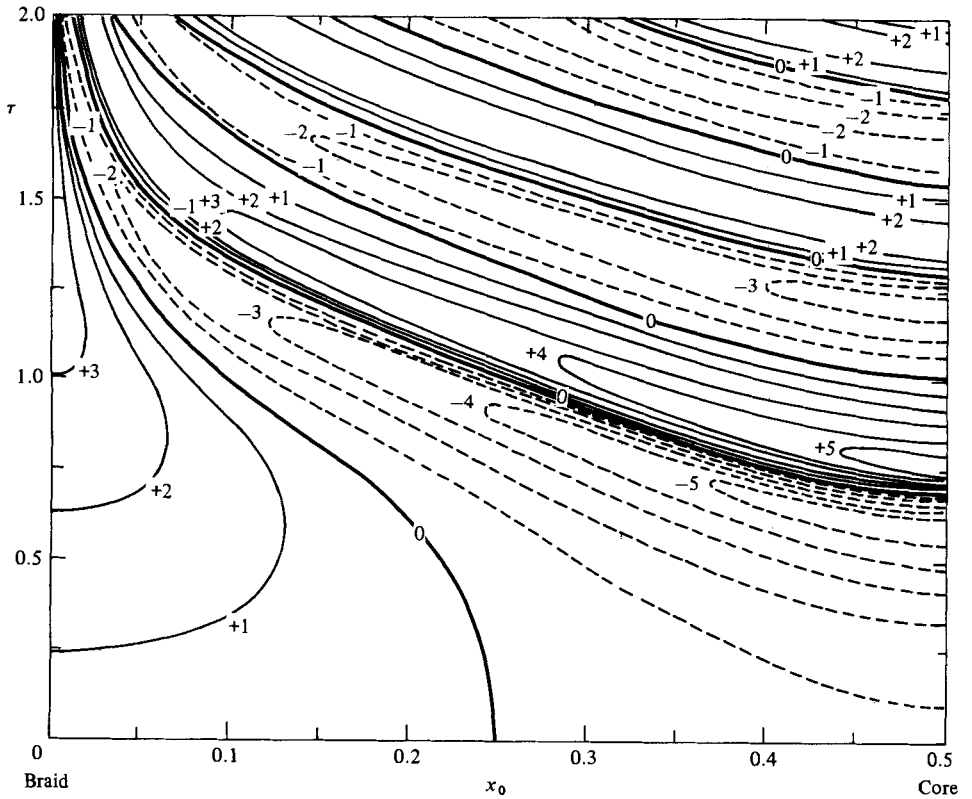

FIGURE 2. The Lagrangian history of the strain along the material interface during roll-up; $\alpha = 0.43$, $Re = 100$. x_0 is the abscissa of an element of interfacial surface at $\tau = 0$. The history of such an element is read vertically upwards. $x_0 = 0$ is the stagnation point; $x_0 = 0.5$ is the centre of the core. The map is symmetric with respect to the right-hand and left-hand margins.

the scalar ρ varies by a fixed amount $\Delta\rho$ anywhere across the diffusion layer, and, where the latter thins out as a result of strain, the magnitude of the scalar gradient correspondingly increases. Analytical models for the vorticity and scalar layers, found in Corcos & Sherman (1976, henceforth called (II)), and in §3.6.5 below, clearly illustrate this difference.

Comparison of the location of the material interface and of the diffusion layers at the same time show that both the vorticity and the scalar layers are accurately centred on the material interface near the saddles, but, for $D/\nu = 1$, cross that surface after it has started winding into a spiral. On the other hand, a fair inference from photographs such as no. 146 in Van Dyke (1982), which show a scalar diffusion layer at a high Schmidt number, is that the much thinner diffusion layer straddles the material interface much more successfully in that case. This issue which bears on the availability of convenient approximate calculations is discussed in §3.6.5.

The nature of the instability. This was discussed and modelled in (II) for a long wave at a finite Richardson number $< \frac{1}{4}$, i.e. with a statically stable but dynamically unstable stratification in a normal gravity field. That discussion (as well as its modification for the shorter relevant wavelengths which are initially more unstable) is applicable in the present case if only the baroclinic generation of vorticity is neglected (set $g = 0$ in (2.18)). It will not be repeated here.

The cat's-eyes and the vorticity distribution. It is clear from figures 3(*a*, *b*) that the

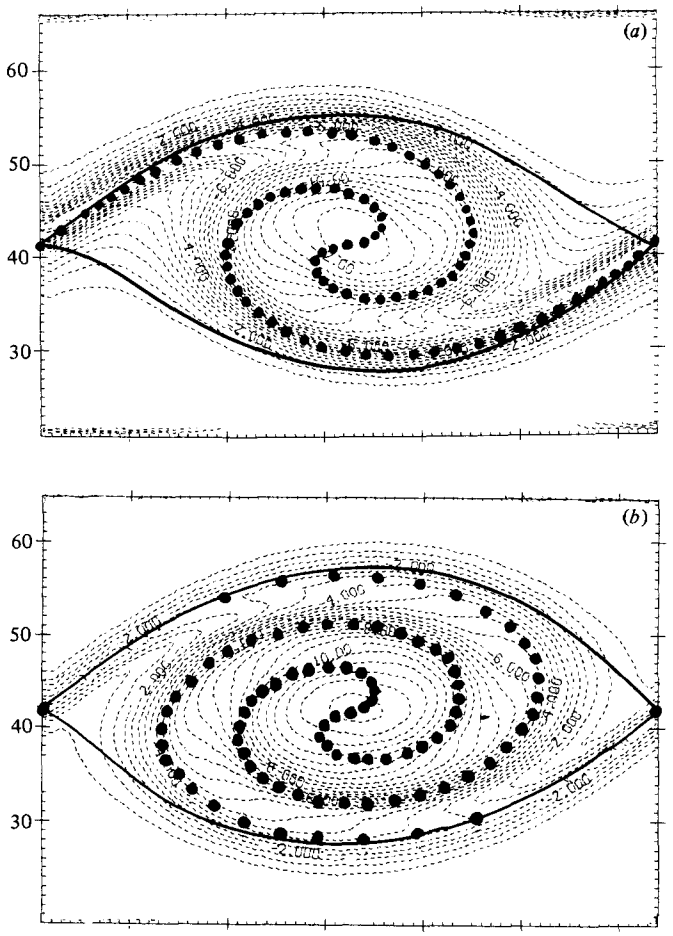

FIGURE 3. Vorticity contours during roll-up; $\alpha = 0.43$, $Re = 100$: (*a*) $\tau = 1.5$; (*b*) $\tau = 2.0$. Interfacial markers and cat's-eye as in figure 1.

area enclosed by the limiting streamlines (the cat's-eyes) grows steadily as a greater fraction of the total vorticity is concentrated within it. The relation between the fraction of fluid volume that recirculates along closed streamlines and the geometric distribution of the fixed amount of vorticity can be made explicit for a simple model, as it was in (II) (equation (3.11)). It is clear that the growth of the cat's-eyes leads to a growth of the displacement thickness of the layer (averaged over the wavelength), and that it can therefore be used as a measure of the growth of the shear layer (see §4.4.1).

3.4.3. *The evolution of the layer beyond the climax state*

Even for an initial Reynolds number Re_i as low as 50, beyond $\tau = 2.0$ the shear across the braids near the stagnation points is less than 5 % of its initial value, and almost all the vorticity is found within the cat's-eyes. This condition may be taken as the effective end of the period of growth for the first phase of the two-dimensional instability.

The layer evolution at later times will be discussed below, but the reader should

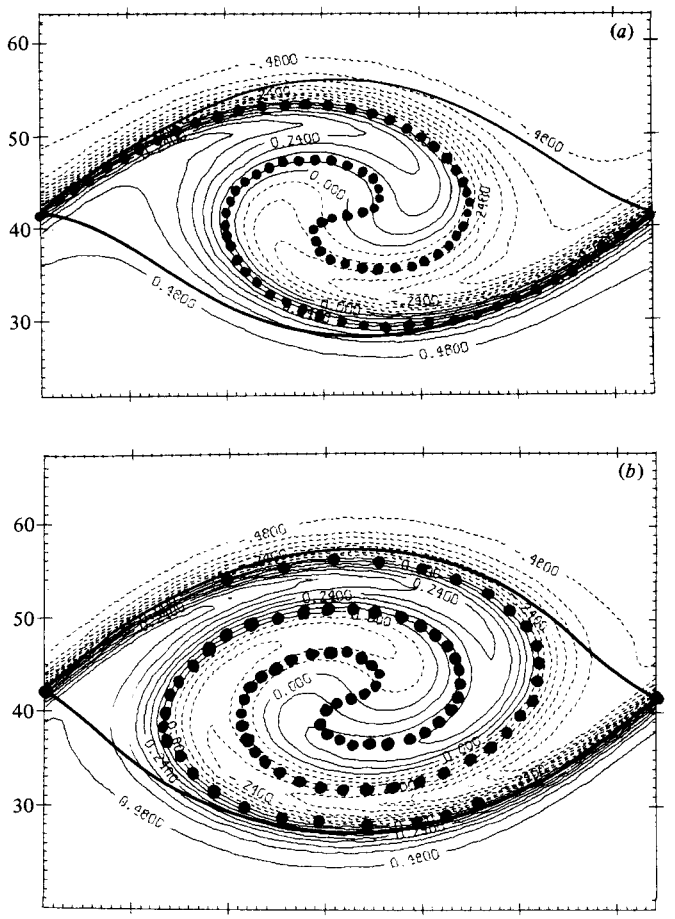

FIGURE 4. Concentration contours during roll-up; $\alpha = 0.43$, $Re = 100$, $Pr = 1$: (*a*) $\tau = 1.5$; (*b*) $\tau = 2.0$; ——, positive or zero ρ; ----, negative ρ.

keep in mind that, as long as the initial conditions include only a perturbation with a single wavelength, that evolution has no correspondence for a real shear layer. For it is around the time of climax and thereafter that the growth of subharmonic perturbations dominates the flow.

Excluding these subharmonic perturbations for the moment, we find that the vorticity distribution characteristic of the climax stage (e.g. $\tau = 2.0$, figure 3(*c*) for the initial amplitude chosen) is not a solution of the steady Navier–Stokes equation. The instability is spent in the sense that the circulation around a cat's-eye has reached a maximum (which approaches the total circulation) and the flow thereafter relaxes: the vorticity is first advected along the closed streamlines which have become almost stationary, but it is also steadily diffused outward across these streamlines. This is illustrated in figure 13 of (I) (for a case with a slight density stratification). The calculation was carried three roll-up times beyond climax. The diffusion causes the vorticity to migrate outside the cat's-eye, and the resulting change in the induced velocity leads to a steady decrease in the thickness of the cat's-eye. Strain and vorticity decrease together.

The same numerical solution shows that, beyond the climax, the vorticity contours

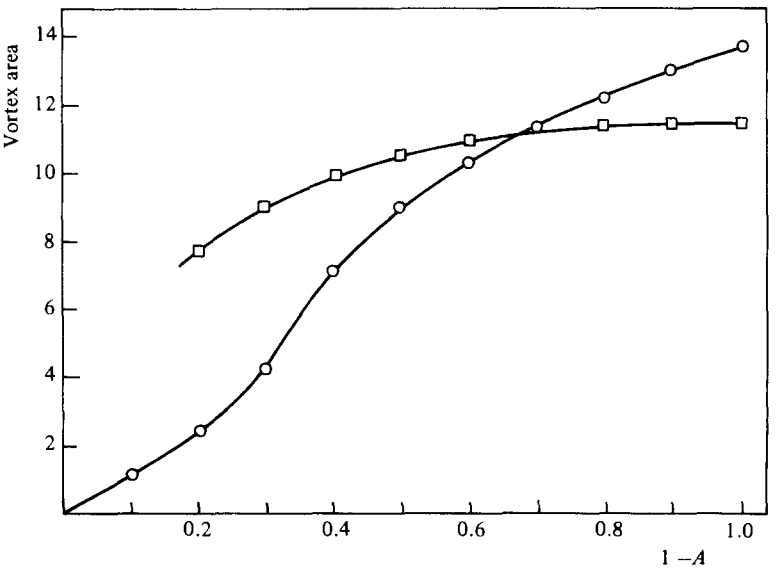

FIGURE 5. The area of Stuart's vortices as a function of the concentration parameter: □, the area bounded by a streamline around which the circulation = 95% of the total circulation; ○, the area on the boundary of which $\Omega = 0.05\Omega_{\max}$.

tend gradually to coincide with the streamlines. If we assume that $\Omega = \Omega(\psi, t)$ and if Γ_c is the circulation around the cat's-eye, the rate of decrease of this circulation, due both to outward diffusion of the vorticity and to the motion of the cat's-eye boundary normal to itself, is given by

$$\frac{d\Gamma_c}{dt} = \nu\left(\frac{\partial\Omega}{\partial\psi}\right)_c \Gamma_c + \Omega_c \frac{dA_c}{dt}, \tag{3.3}$$

where Ω is the vorticity, c refers to the cat's-eye boundary and A_c is the area that it encloses.

An accurate solution of (3.3) would require a faithful model of the relaxing vorticity and strain distributions, but there is little doubt that asymptotic solutions can be constructed with the help of linear viscous stability theory after a sufficient fraction of the vorticity has diffused out of the cat's-eye.

Pierrehumbert & Widnall (1981) argue that it is impossible for a rolled-up shear layer to relax forever in the way described above. Their hypothesis, first suggested by Moore & Saffman (1975), is inferred from the properties of a particular family of stationary inviscid z-wise-periodic vorticity distributions. These have the same wavelength and circulation per wavelength. In addition their vorticity is uniform: 'The vortex area...reaches a maximum at a ratio of (vortex width to spacing) $w = 0.87$.... The existence of an upper bound for the vortex area confirms the basis of the tearing mechanism for shear-layer growth. If a vortex is initially characterized by a value of $w < 0.87$, turbulent entrainment of irrotational fluid will cause it to evolve in the direction of increasing area until the area maximum is reached. At this point there is no longer a nearby steady state with greater area...unless the vortex spacing is allowed to increase. Presumably then, the vortex breaks up...'

But the argument seems to require that the relaxation take place by (laminar or

turbulent) diffusion through a set of steady-state inviscid solutions, and indeed through the very special one which these authors studied. For instance, the Stuart (1967) solutions of the steady Euler equation,

$$\psi = Uk^{-1} \ln (\cosh kz + A \cos kx), \tag{3.4}$$

where ψ is the stream function and $k = 2\pi/\lambda$ is the wavenumber, do not share this property. If we define the area of the Stuart vortex layer as either that round which the value of the circulation is $\Gamma_c = b_1(4\pi U/k)$, or, on the boundary of which $\Omega = b_2 \Omega_{\max}$, where $b_2 = 1 - b_1 = \epsilon \ll 1$, we find as shown on figure 5(*a*, *b*) that the area occupied by the vorticity increases monotonically as A decreases to zero, i.e. as vortices merge and as the layer loses its periodicity and becomes a simple shear layer. Thus the property required for the authors' hypothesis is not even shared by all stationary inviscid periodic solutions. In any case, the non-existence of such solutions does not in general imply the non-existence of viscous and damped soutions.

For instance in the linearized stability problem for the shear layer, there are no inviscid eigenvalues of any kind for $\alpha > 1$, but there are eignevalues of the viscous problem which correspond to damped waves, no matter how thick is the layer next to the wavelength. For high Reynolds numbers, some of these are in fact valid asymptotic solutions of the nonlinear relaxation problem for large times. The final asymptotic state must be that of the simple shear layer, i.e.

$$u = U \operatorname{erf}\left\{\frac{z}{(4\nu(t-t_0))^{\frac{1}{2}}}\right\},$$

where the new time origin $t_0 < 0$.

In summary, if only one unstable perturbation wavelength is initially present, the subsequent roll-up, by hastening diffusion, ultimately serves to increase the non-dimensional wavenumber in such a way as to insure the decay of the perturbation. If a real shear layer has a different dynamical history, it is, as we shall see, because it becomes preferentially unstable to a sequence of perturbations of increasing wavelengths, and not, as Pierrehumbert & Widnall suggest, because the relaxation by diffusion of the original roll-up is incompatible with the equations of motion.

3.5. *The second stage of instability in the two-dimensional shear layer: subharmonic growth and pairing*

The study of the nonlinear stages of the first instability has led us to the following conclusions, which taken together offer strong hints about the general nature of the flow in a shear layer whose rapid growth rate is unabated in time or downstream.

(*a*) The result of the first instability is the temporary concentration of the vorticity into separate lumped vortices.

(*b*) Each one of these finite vortices creates, and on the whole is contained by, a region within which streamlines are closed and the process of concentration as long as it lasts leads to an increase of the area of these regions with time. During their growth, fluid that was streaming on either side of the layer is therefore diverted so that it becomes solicited by velocity along newly formed closed streamlines. Thus, as long as the cat's-eye boundary expands, there is a systematic flux of fluid across it from the outside inward.

(*c*) The layer growth that is observed with the help of an optically visible passive scalar initially coincident with the vorticity is caused by the growth of the cat's-eye

area within which the scalar is almost completely constrained to recirculate. This is discussed in greater detail by Jimenez (1980) and Jimenez, Martinez-Val & Herman (1981).

(*d*) Vorticity concentration and the initial layer growth associated with the roll-up could not occur if many waves of different phases and/or different lengths grew simultaneously in the same region of the shear layer: since they would have to share the fixed amount of vorticity, $2U$ available per unit length of layer, the circulation around each lump would be correspondingly diminished and so would the total area of the cat's-eyes, and the layer thickness. Therefore, in order for a layer to approach its maximum possible growth rate, a single wave must be able to grow by itself within the space of its own length, and for the time required for one roll-up. If the initial conditions are made of a continuous spectrum of random perturbations, either the concentration and growth associated with the roll-up will not occur or a selection must operate that allows waves to grow one at a time. This implies that the dynamics of vigorous growth cannot be incoherent over times comparable to a concentration time, i.e. at least of order λ/U or over lengths at least of order λ.

(*e*) Finally, according to our previous discussion, the concentration of vorticity caused by a single wave is a temporary event, after which the vorticity once again is spread uniformly in the streamwise direction.

Now there is still a vigorous controversy among experimentalists (e.g. Dimotakis *et al.* 1981; Hussain & Clark 1981) about the later fate of spanwise vorticity. This lack of agreement is certainly due in part to the difficulty of measuring dynamically relevant quantities in a way that must not require averaging of partially stochastic functions, and thus their integration either in space or time. We will eschew a comprehensive discussion of these experimental findings, which would involve us in many collateral issues. But the most discriminating and therefore the most persuasive evidence such as that of Browand & Troutt (1980), Browand & Ho (1983) and of Jimenez *et al.* (1981) lends strong support to the thesis that spanwise vorticity after roll-up is concentrated by coalescence into even larger, quasi-two-dimensional distinct vortices at all Reynolds numbers investigated.

We now enquire how coalescence of vorticity occurs after roll-up, and defer to Part 2 theoretical support for the conclusion that this coalescence is preferentially two-dimensional.

3.5.1. *Subharmonic growth*

Early observations of the natural or forced transition of a free shear layer (Sato 1956; Wille 1963; Freymuth 1966; Browand 1966) indicated that the dominant frequency of passage of disturbances within a shear layer decreases, usually by a factor of 2, as the observation point was moved downstream. Kelly (1967) gave a mathematical model of the initiation of this further modification of the flow. He constructed an approximate representation of the climax state of the previous or first stage by superposing on a mean shear the eigenfunctions of the original linear problem, which are periodic with wavelength λ and are given a finite amplitude. He then added to this composite flow a small (subharmonic) perturbation with wavelength $n\lambda$ and a particular phase relation to the first wave. He found that such perturbations could grow rapidly, that their growth rate depended on the amplitude of the primary perturbation and that the growth rate was a maximum when $n = 2$. More recently, Pierrehumbert & Widnall (1982, see also part 2) performed a similar analysis, but starting with a steady base flow which is the Stuart solution (3.4) already discussed, for selected values of the parameter A, and treating the linear stability of this flow

as a two-dimensional eigenvalue problem. Both found that a perturbation with a wavelength twice that of the fundamental (the wavelength of the finite wave in Stuart's solution) can grow faster than it would if the latter were absent† and that the initial growth rate of that subharmonic increases with the concentration of the vorticity of the fundamental.

3.5.2. *Coalescence*

This subharmonic instability is initially somewhat similar to the instability of a row of point vortices studied by von Kármán (see e.g. Lamb 1932), but the outcome is different. In the case of vortices of finite area, numerous experiments suggest that there occurs a coalescence of vorticity so that stronger, fewer, more distant vortices replace the previous distribution. Details are given in Brown & Roshko (1974), Winant & Browand (1974), Koop & Browand (1976), Jimenez *et al.* (1981), Ho & Huang (1982) and several others.

Although the question is worth further study, it seems likely, on the basis of the work of Kelly (1967), of the treatment of Roshko's data by Jimenez *et al.* (1981) and of the arguments presented above, that, of all the longer waves that can interact with a given fundamental, only subharmonics offer the possibility of vigorous growth. We have thus taken, as a prototype of a more comprehensive initial perturbation, one which is made up of that wave to which linear theory ascribes the maximum initial growth rate together with a sequence of its subharmonics.

The bulk of our numerical simulations with composite initial perturbations was performed with initial conditions which include only a fundamental and its first subharmonic. Two cases were also calculated for which the fundamental, first and third subharmonics (i.e. λ, 2λ, 4λ) were included. F. S. Sherman (unpublished) also studied a few additional cases such as the interaction between waves with lengths in the ratio $\frac{1}{2}$ to $\frac{1}{3}$ on a grid which accommodated two of the first kind and three of the second. In all cases investigated, the interaction is such as to lead to the eventual dominance of the longest wave allowed by the grid. The path taken by the interaction depends on the relative initial amplitude and phase of the waves of different lengths which have been simultaneously introduced and on their initial growth rate (according to linear theory).

3.5.3. *The response of the layer to a fundamental and a first subharmonic*

Both perturbations are introduced for $t = 0$ and both are eigensolutions of the linear stability problem. In some cases, the eigenfunctions are obtained by solving the viscous (Orr–Sommerfeld) equations, in some cases by solving the linear inviscid equations. These differ little, and it was verified that the subsequent numerical solutions of the nonlinear viscous problem are undistinguishable after a few time steps.

Initial growth. On figure 6 (drawn from older calculations for a moderately stratified shear layer) are plotted as a function of time the height of the cat's-eye for the composite wave and the integral over the left-hand half of the grid of the velocity component w, both when the subharmonic grows alone and when it grows together with the fundamental. Note that, since the fundamental is periodic over the half-grid length, one may consider this integral as a measure of the amplitude of the subharmonic alone. It will be noticed that, when the initial amplitude of the disturbance is sufficiently small, the initial growth rate of the subharmonic is unaffected by the presence of the fundamental, as linear theory predicts. Later, the

† But see Brachet & Orszag (1982).

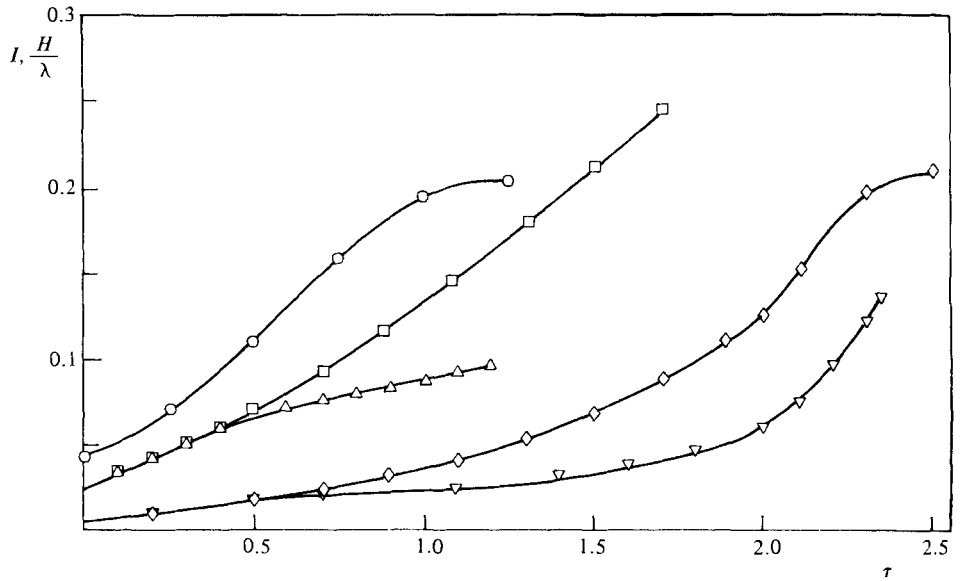

FIGURE 6. The early inhibition of the subharmonic by the fundamental; $\alpha_1 = 0.215$, $\alpha_2 = 0.1075$, $g\Delta\rho(2k_1\rho_0 U^2)^{-1} = 0.219$. ○, H/λ for short wave alone. Other symbols denote integral of w over half-length of grid: □, long wave alone; △, long wave in presence of short wave, amplitude ratio $a_2/a_1 = 1$; ◇, long wave alone; ▽, long wave in the presence of short wave with $a_2/a_1 = \frac{1}{4}$.

growth rate of the subharmonic is inhibited though not suppressed by the presence of the fundamental. The same figure shows that the length of time during which the fundamental succeeds in inhibiting the growth of the subharmonic depends on their relative amplitude. In fact if the initial subharmonic amplitude is sufficiently large that wave grows preferentially and dominates the interaction from the start.

In the bulk of the calculations presented, the initial ratio $\mathscr{A}$ of the amplitude of the subharmonic to that of the fundamental is 0.5.

The effect of the relative phases of the two perturbations. In (I) it was demonstrated that the relative phase of the two perturbations bears on the course of their interaction. Riley & Metcalfe (1980 and personal communications) have provided more detailed evidence. There are two typical phases. If the initial stream function of the fundamental is

$$\psi_1 = \phi_1(z) \exp \mathrm{i}\alpha x,$$

then the two typical phases for the subharmonic are

$$(a) \quad \psi_2 = \phi_2(z) \exp \tfrac{1}{2}\mathrm{i}\alpha x \tag{3.5a}$$

or

$$(b) \quad \psi_2 = \phi_2(z) \exp \tfrac{1}{2}\mathrm{i}(\alpha x \pm \pi). \tag{3.5b}$$

In case (a) the initial effect of the long wave is to displace up and down those nodes of the short wave that become centres of accumulation of vorticity. This leads to the rotation of pairs of vortices one around the other and through their coalescence to new vorticity concentrations within cat's-eyes whose length has doubled. In case (b) the contribution of the long wave is instead to modulate the strength of the short-wave vortices. The strain field created by the stronger vortices elongates the weaker ones and slowly extrudes them so that the vorticity of the weaker vortices migrates

diagonally towards the stronger ones along newly forming braids. During this interaction it appears that the bulk of the migrating vorticity escapes the closed streamline region, so that the circulation around the surviving vortices is not considerably enhanced, the strain along the new braids is relatively weak, the interaction is slow (on the scale of λ_1/U), the cat's-eyes are elongated, and most of the vorticity is spread in the streamwise direction just outside the cat's-eyes.

For phase relations that are neither (*a*) nor (*b*), Riley & Metcalfe show that pairing occurs. The linearity of the initial problem indicates that such a case is initially merely the superposition of cases (*a*) and (*b*), so that one would expect case (*a*) to dominate such an evolution after a time which depends on the proximity of the phase angle to $(n+1)\pi/\alpha$. For this reason we expect the flow to be dominated by pairing (phase *a*) interactions, and we have chosen phase (*a*) in our numerical simulations. But, for the same reason, we would expect that a natural layer amplifying selectively a spectrum of ambient subharmonic perturbations of random phases should grow less rapidly than one which is supplied by a sequence of subharmonics whose relative phase angle is given by (3.5*a*).

Streamlines, vorticity, material interface and deformation during pairing. In figures 7(*a–f*) streamlines and interfacial markers are shown, while vorticity contours are given in figures 8(*a–c*). The presence of the subharmonic perturbation and the slight concentration of vorticity which it implies at the centre of the grid prevent the two cat's-eyes from closing there. As time increases, one notices that the two interfacial spirals approach each other as they rotate around the point of polar symmetry, and that the rate of stretching of the interface is particularly large in that region: this is the result of the enhanced deformation induced by the two vortices as they approach each other. Later (figures 7*e,f*), the configuration of the interface becomes quite complex. For $\tau = 3$ all thirteen folds of the material interface that cross the x-axis seem to be oriented and stretched in almost the same direction, suggesting that the deformation field at a given time is reasonably uniform over a large area which covers the two vortices. Its principal axis of positive strain is inclined to the line joining the two vortices by an angle which, one guesses, approaches 45°, and the vorticity distribution for both vortices is itself strongly affected by this strain field.

From our calculations for an initial Reynolds number of 100 or even 50, vorticity diffusion, even though considerably enhanced between the vortices by the large strain, does not destroy rapidly the individual identity of the two vortices which are pressed against each other. Thus, even a substantial time after the new cat's-eye has reached its maximum area, the interdiffusion of the two vortices is only partial (see e.g. figures 8*a, b*). As a result, their precession around each other continues, and the deformation field created by the two joined vortices rotates along with the line joining the two vortex centres. The strength of this part of the deformation field evidently depends on the extent to which the two vortices remain distinct, and therefore on the degree of diffusion of the vorticity. As a result, one expects the two vorticity distributions to be more elongated along the rotating axis of principal strain for higher than for lower values of the Reynolds number. This is confirmed by calculations. For the inviscid cloud-in-cell calculations of Christiansen (1973) for a periodic array of identical initially round vortices (which coalesce if the ratio of their initial radius to spacing is sufficiently large) the elongation suffered by the two vortices is strikingly large.

The braids issued from the two remaining stagnation points (at the left and right margins of the grid) are almost completely depleted of vorticity. They are also accurately bisected by the material interface until climax.

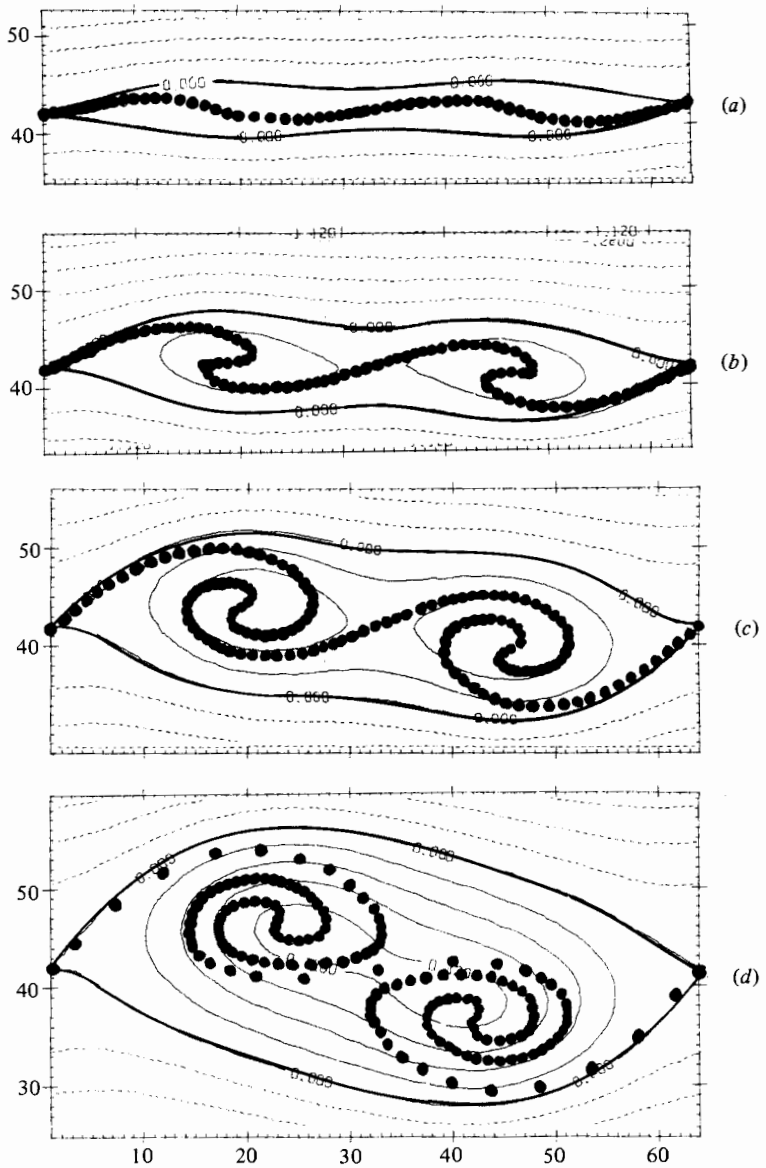

FIGURE 7 (*a–d*). For caption see facing page.

We have calculated the strain rate along the complete interface as a Lagrangian function of time, using, as shown on figure 7 (*a*), markers whose initial location anticipated their future migration in order to retain later a reasonable marker density. In spite of these precautions, towards the end of the calculation (figure 7*f*), the extraordinary variation in the stretching history of different parts of the interface left us with excessively distant markers.†

† In addition we found the trajectory of the crowded initial population of markers near the surviving stagnation point to be quite sensitive to small errors in their initial velocities.

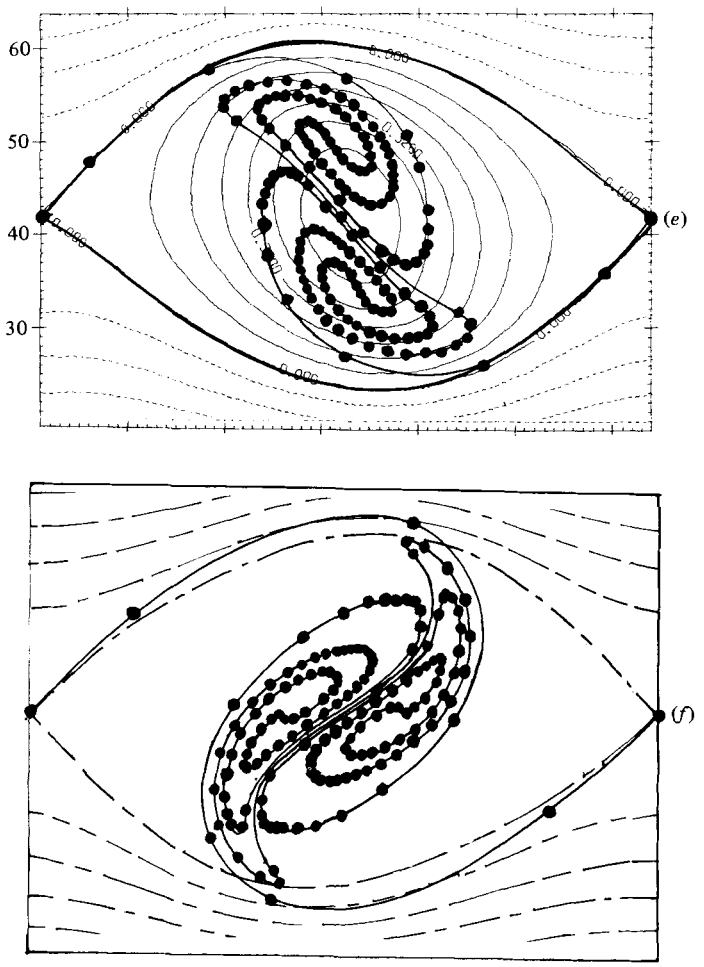

FIGURE 7. Roll-up and pairing: streamlines and material interface; $\alpha_1 = 0.43$, $\alpha_2 = 0.215$, $Re = 100$. The heavy line is the cat's-eye. The dots are interfacial markers. These have been connected for clarity in (*e*,*f*), and in (*f*) the circular streamlines inside the cat's-eye have been deleted. The cat's-eye is a broken line. (*a*) $\tau = 0.5$; (*b*) 1.0; (*c*) 1.5; (*d*) 2.0; (*e*) 2.5; (*f*) 3.0.

The scalar ρ. The distribution of the passive scalar ρ is shown on figure 9. It is relevant both to the important problem of molecular mixing and to the dynamical inferences which can be drawn from instantaneous experimental realizations of optically visible properties of the flow (e.g. Brown & Roshko 1974; Breidenthal 1978; Hussein 1981). Evidently the scalar diffusion pattern like the vorticity is influenced by the strain field, but the difference between the boundary conditions governing vorticity and density lead to important differences in their distribution, as already noted in §3.4.2. During pairing the braids continue to be regions of maximum density gradient in which the gradient layer thickness is simply governed (see §3.6.5) by the history of the interfacial strain and by the diffusivity. On the other hand, within the area that includes the two merging cores, the gradients are quite diffuse, the concentration is reasonably uniform and gives little direct evidence of the existence of the large intervortical strain. In addition one would be hard pressed to distinguish

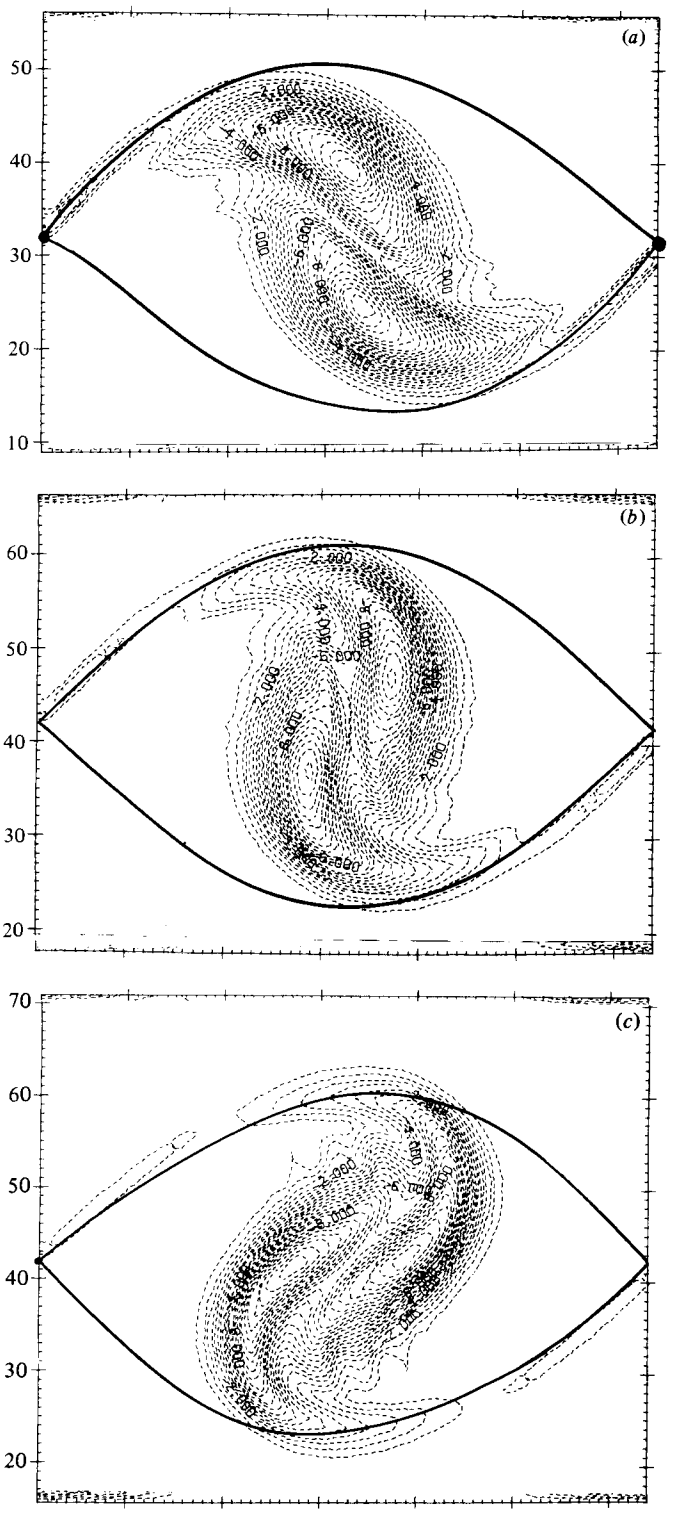

FIGURE 8. Contours of constant vorticity and cat's-eye during pairing; $\alpha_1 = 0.43$, $\alpha_2 = 0.215$, $Re = 100$: (*a*) $\tau = 2.5$; (*b*) 2.75; (*c*) 3.0.

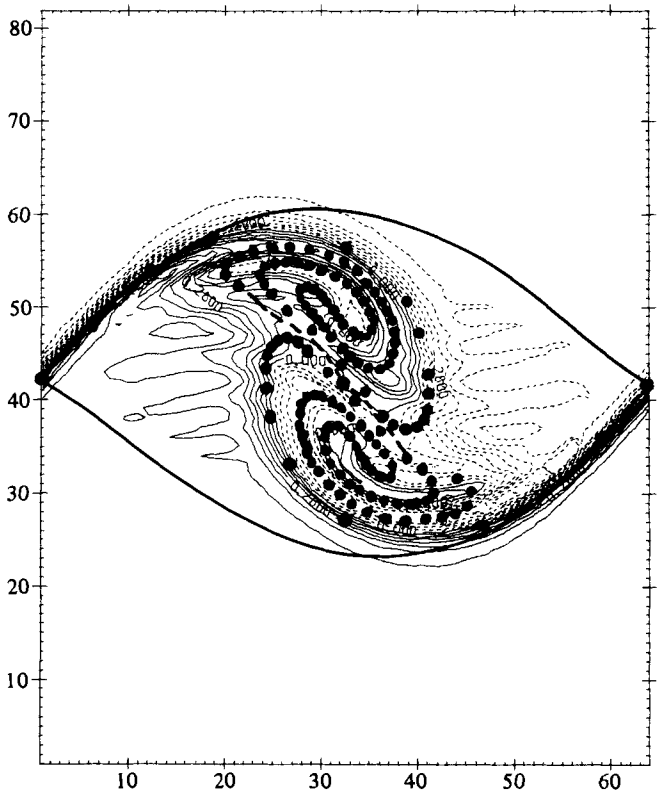

FIGURE 9. Contours of the scalar ρ during pairing; $\alpha_1 = 0.43$, $\alpha_2 = 0.215$, $Re = 100$, $Pr = 1$, $\tau = 2.5$. Dotted lines indicate negative values of ρ.

the separate outlines of the two merged cores. Thus the magnitude of the density gradient is largest in the braids and small in the cores, whereas the value of the spanwise vorticity is largest in the cores and very small in the braids. As a result, optical techniques based (like that of Brown & Roshko 1974) on the distribution of a passive scalar with the same boundary conditions as those used here do not yield direct information about vorticity concentration and must be interpreted with care.

Nevertheless, they have played a major role in the discovery of coherent structures and they are useful in assessing whether and how closely a purely deterministic and two-dimensional model of coalescence is similar to the evolution of real coherent structures. For instance figure 10 compares a famous spark-shadowgraph by Roshko (1976) of a part of a mixing layer to our constant-density contour plots at $\tau = 3$. The resemblance is striking and all the more significant because the two flows are different in several respects:

(*a*) The real flow is an S-layer, the calculated flow a T-layer;

(*b*) The event photographed is a fourth pairing, while that calculated is a first pairing;

(*c*) The local Reynolds number in the real flow is a hundred times larger than in the calculated flow. In addition, for the real flow, the photographic contrast is related to a spanwise average of the Laplacian of the index of refraction, a quantity which is equivalent to the Laplacian of ρ, while the pattern in the calculated flow is that created by the magnitude of the gradient of ρ.

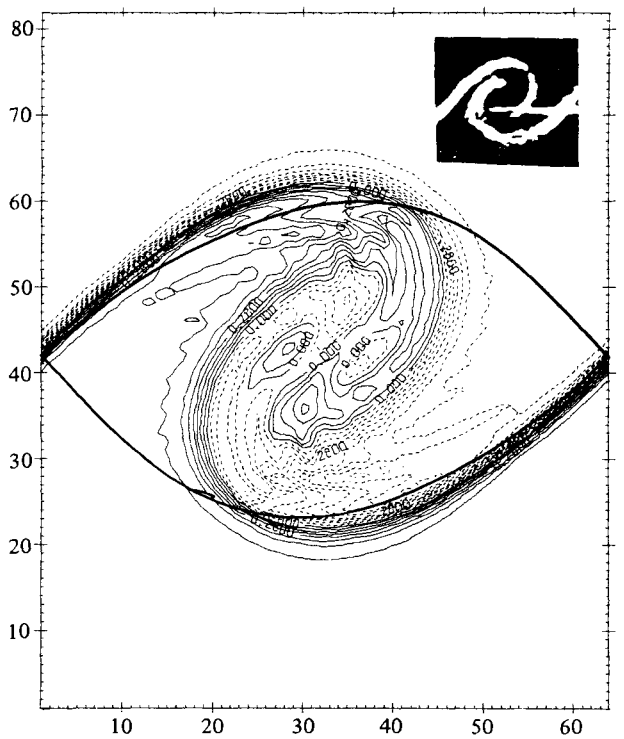

FIGURE 10. Contours of the scalar ρ for the same case; $\tau = 3.0$. Insert is shadowgraph from Roshko (1976).

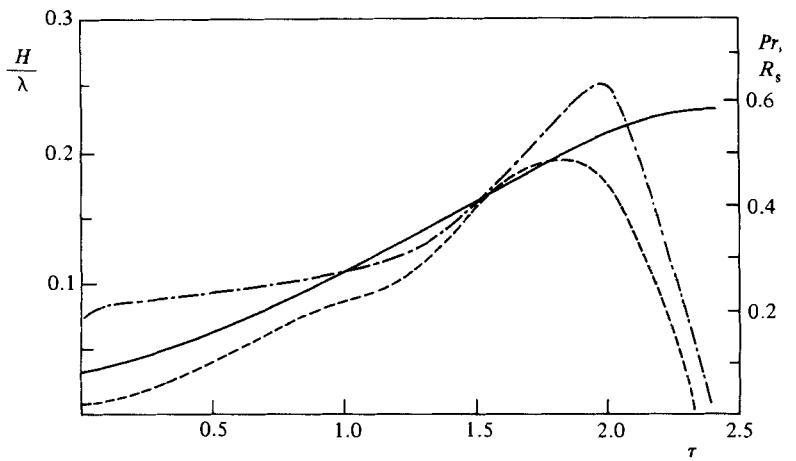

FIGURE 11. The cat's-eye semiheight H/λ (——), the integral of the Reynolds stresses (— · —), and the rate of production of kinetic energy (– – –) during roll-up and pairing.

Thus the comparison suggests that the presence of three-dimensional modes of motion does not seriously alter the spanwise average of the large-scale evolution of the layer, that successive pairings have a great resemblance to each other, and that the streamwise development of the mixing layer is similar to the development in time.

Reynolds stress. For a flow that evolves as a discrete row of isolated vortices, it seems particularly inappropriate (though traditional) to ascribe any physical significance

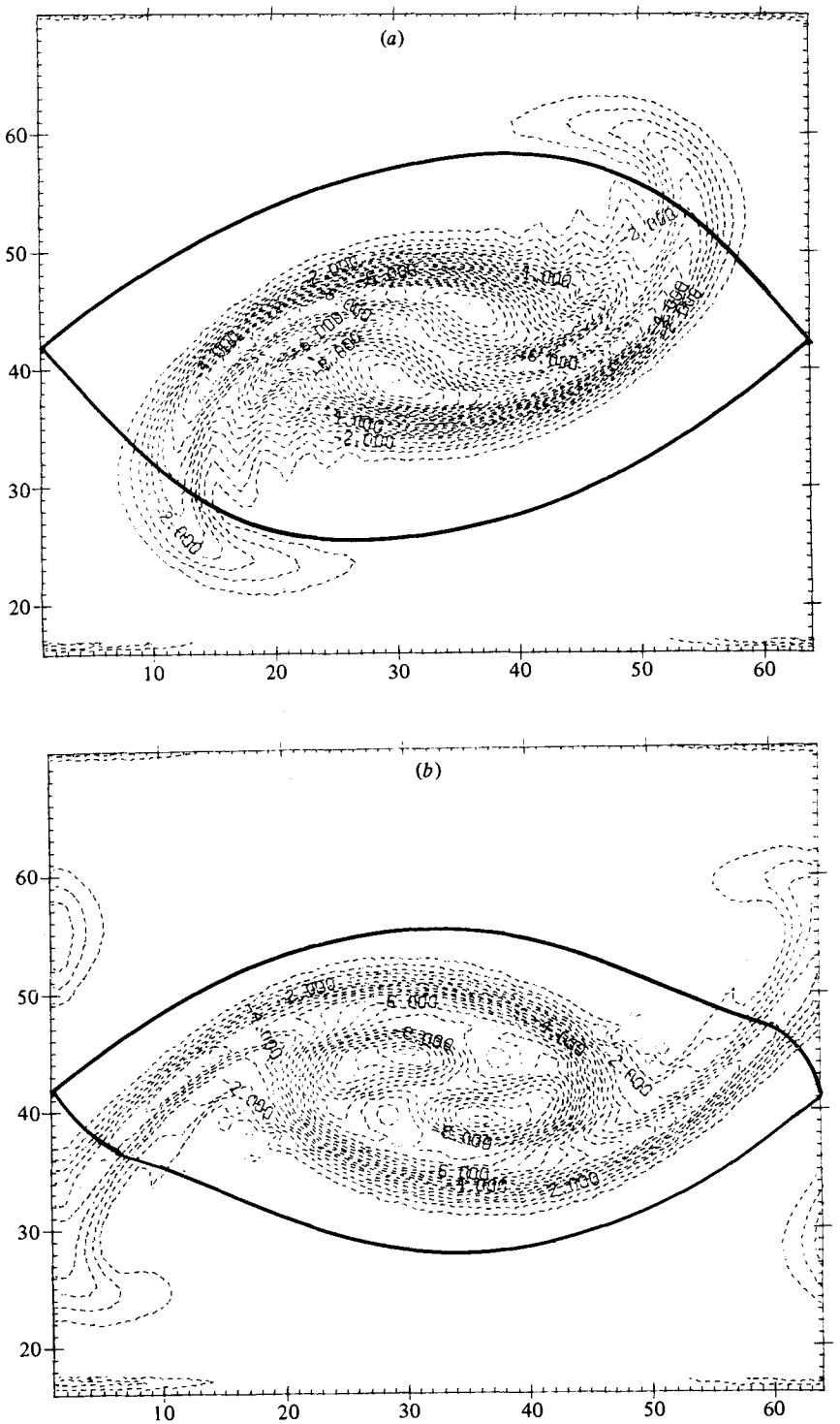

FIGURE 12. Late stages of pairing: vorticity contours and cat's-eye: (*a*) $\tau = 3.75$; (*b*) $\tau = 4.0$.

to a mean (i.e. here x-averaged) flow and to its interaction with a perturbation field; such an artifact can only obscure the dynamical events that govern the flow's evolution. Nevertheless, this point of view continues to be influential and is the motivation for numerous measurements of Reynolds stress. The concentration of vorticity into vortices of increasing size and the corresponding increase in the lateral extent of the flow wherein the velocity substantially differs from its mean loosely imply that perturbation energy grows during pairing, so that according to the traditional interpretation a large amount of work should be done by the Reynolds stresses upon the mean flow during that time. This 'energy-production' term can be calculated from the results of the numerical simulation as a function of time for a roll-up and for a roll-up and pairing. It peaks almost precisely with the rate of growth of the cat's-eye area and in the absence of a new pairing vanishes with it (figure 11). The integral of the Reynolds stresses reaches a maximum when the centres of the two vortices lie on a line at an angle of roughly $\frac{3}{4}\pi$ from the positive x-axis. On these points, the correspondence between the computations and the measurements of Browand & Weidman (1976) is excellent.

The late stages after a first pairing. Figures 8(*c*) and 12(*a*, *b*) show that, in the absence of a second subharmonic, the precession of the two coalesced vortices and of the associated strain field leads to rather complicated motion of the vorticity during which a fraction of this vorticity is thrust outside the cat's-eyes. Coalescence, accordingly, is not complete. Similar results have been discussed by Overman & Zabusky (1981) in connection with inviscid calculations of pairing. Apparently, integral invariants of the moment of the vorticity distribution (see e.g. Batchelor 1967) require this dispersion. It can be seen from figures 8(*c*) and 12(*a*, *b*) that, kinematically speaking, the escape of vorticity is achieved when the cat's-eye shrinks as a result of the precession of the two paired vortices, leaving some of the vorticity in the streaming part of the flow. It is then advected to the right and left of the cat's-eye. In the inviscid calculations mentioned above, the vorticity that escapes coalescence is filament-like. Numerical simulations with successive pairings show that the stray vorticity caused by one pairing is drawn back into the braids during the next pairing and subsequently finds its way back to the core. The dynamical importance of this source of braid spanwise vorticity has not yet been assessed.

3.5.4. *Second subharmonic interaction*

In one case a fundamental and two subharmonics were initially introduced. The wavenumbers were $\alpha_1 = 0.43$, $\alpha_2 = 0.215$ and $\alpha_3 = 0.1075$ and the grid was correspondingly enlarged. The amplitude ratios were $\mathscr{A}_1 = 0.5$; $\mathscr{A}_2 = 0.25$. The evolution of the two subharmonic interactions was sequential and very similar. For $\tau < 1.50$ the presence of the second subharmonic could only be detected, say, on streamline plots by a very slight vertical displacement (up on the left and down on the right) of the individual cat's-eyes associated with the first subharmonic as well as by a slight increase in the initial rate of growth both of their areas and of their maximum thickness (figure 13). Similarly, the rate of growth during roll-up is somewhat enhanced by the presence of a first subharmonic.

The timescale for the final pairing is very nearly twice that for the previous one, and the cat's-eye area at final climax is also very nearly twice that of the two cat's-eyes at the climax of the first subharmonic for a single pairing.

On the other hand, full similarity between first and second pairing would require that, say at climax, the value of the vorticity be halved at corresponding points. In

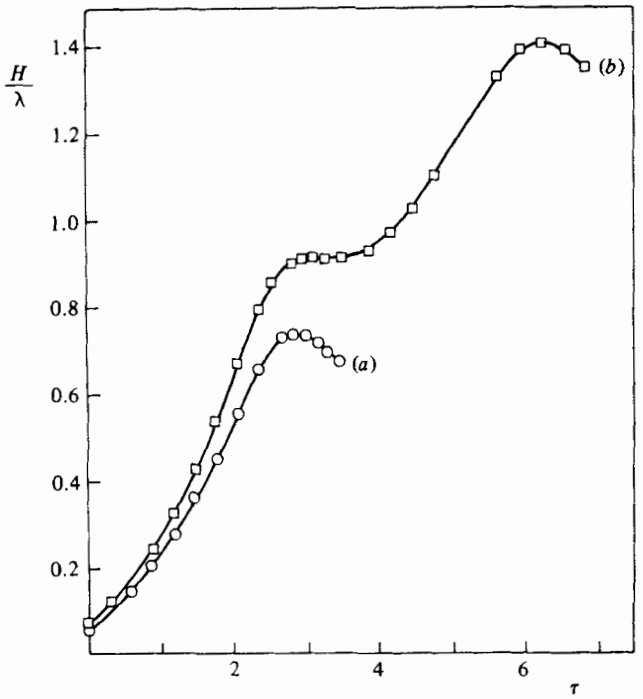

FIGURE 13. The growth rate of the cat's-eye semiheight H; $Re = 100$: (*a*) one pairing, $\alpha_1 = 0.43$, $\alpha_2 = 0.215$; (*b*) two pairings, $\alpha_1 = 0.43$, $\alpha_2 = 0.215$, $\alpha_3 = 0.1075$. The amplitude ratios are $a_2/a_1 = 0.5$ and $a_3/a_1 = 0.25$.

fact, at second climax the maximum vorticity is 9.8, while at first it is 11.8. Vorticity must decrease by molecular diffusion, and the diffusion rate is evidently slower than the rate of growth of the cat's-eye area (i.e. the entrainment rate). Therefore there is only an approximate similarity between successive pairings.

3.6. *General properties*

3.6.1. *Rate of growth*

The growth rate of the T-layer may be defined in several ways. We may for instance use as a measure of lateral scale at any time the semiheight H of the cat's-eye, the cat's-eye area A_c divided by its wavelength, or other integral properties such as

$$\delta_\omega = UL^{-1}\int_0^L \left(\frac{\partial u}{\partial z}\right)_0^{-1} \mathrm{d}x,$$

where the slope $\partial u/\partial z$ is evaluated at $z = 0$, or again

$$\theta = L^{-1}\int_{-\infty}^{\infty}\int_0^L \left[1-\left(\frac{u}{U}\right)^2\right]\mathrm{d}x\,\mathrm{d}z,$$

respectively the vorticity thickness and the momentum thickness. These various measures of thickness are shown on figure 14. None is monotonic in τ, but δ_ω has a particularly pronounced and narrow peak around $\tau = 2.25$.

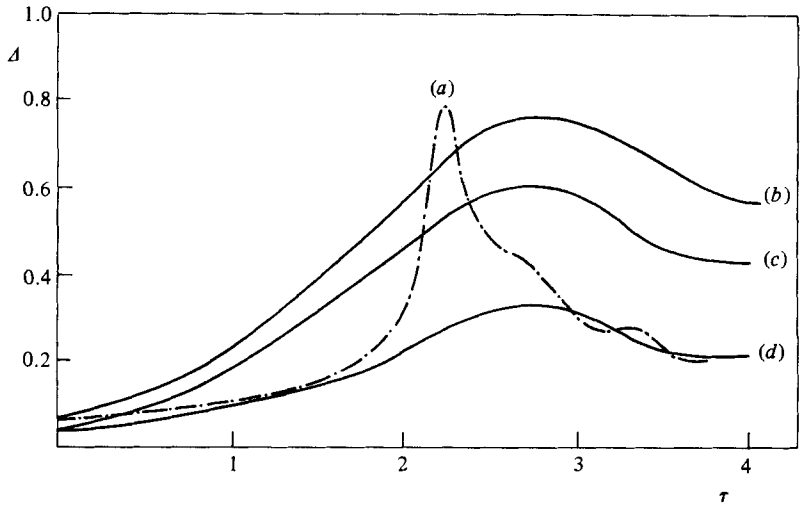

FIGURE 14. Four thickness scales as functions of time for roll-up and pairing; $\alpha_1 = 0.43$, $\alpha_2 = 0.215$, $Re = 100$: (*a*) δ_ω, vorticity thickness. (*b*) $\overline{H}$, cat's-eye area; (*c*) H, cat's-eye semiheight; (*d*) θ, momentum thickness.

In a random version of the layer, one would expect the location of this peak in time (for a T-layer) or in x (for an S-layer) to be distributed around some mean location for each pairing as suggested by the measurements of Brown & Roshko (1974). In these measurements the statistical location of any event associated with a given pairing is distributed over a distance comparable with the distance between two consecutive vortices. Nevertheless, it is not clear that the measurements at a stationary streamwise station of a time-averaged value of δ_ω should increase linearly with streamwise distance x instead of oscillating around this smoothed growth curve. Thus measurements of δ_ω made at regular intervals might appear to have a measure of scatter or uncertainty and the momentum thickness might be preferable to characterize the growth rate of an experimental layer. Even this choice may not eliminate apparent scatter (see Browand & Latigo 1979).

3.6.2. *Comparison between calculated and experimental growth rates*

It is of great interest, as implied at the beginning of §4, to compare smoothed growth rates provided by our deterministic two-dimensional calculations with observed time-averaged growth rates. This has been done for limited times (i.e. through one pairing) by Riley & Metcalfe (1980). But as already noted, the calculated growth rates in the T-layer depend on the imposed ratio of initial subharmonic amplitudes. This dependence is unnatural to some extent, since it is a consequence of the parabolic form of the problem for the T-layer. In the S-layer the upstream conditions are only partially controlled by the experimentalist, since the mixing-layer vorticity induces upstream perturbations which are probably not negligible next to those which would in any case be advected along and past the splitter plate. Laufer & Mankovitz (1980) and Jimenez (1980) have considered this problem theoretically. The latter, in particular, has evaluated the perturbation field created upstream by an idealized pairing and inferred a minimum growth rate. But the idealization used may not be adequate to ensure accurate answers. Thus it is not yet known on theoretical grounds whether this feedback effect is strong enough to control the rate of pairing and growth

independently of the level of turbulence found upstream of the splitter plate.† On the other hand, it seems clear that as $\Delta U/\overline{U}$ decreases the S-layer becomes more strongly parabolic (see e.g. Corcos 1981), the spacing between all vortices increases, their mutual induced field correspondingly decreases and upstream boundary conditions must reappear as external parameters.

3.6.3. *Entrainment*

The word entrainment normally connotes the rate at which irrotational fluid which had been part of the non-turbulent streams on either side of the mixing layer becomes part of the layer. An assumption underlying many older discussions of entrainment following the work of Corrsin & Kistler (1954) had been that entrained fluid became turbulent, i.e. acquired vorticity upon crossing an irregularly shaped and unsteady but continuous surface or very thin layer which constituted a boundary between turbulent and non-turbulent flow. There is no compelling reason to assume that fluid ingested in the turbulent region acquires almost discontinuously a finite amount of vorticity, and we find it useful to separate the concept of entrainment from that of mixing. In our deterministic two-dimensional layer, entrainment can be defined with some precision.

During the initial roll-up and the successive pairings, the concentration of vorticity within compact regions around which circulation increases monotonically results in the increase of the volume occupied by the cat's-eyes, i.e. of the volume of fluid that recirculates or whose streamlines are, at any time, closed on themselves. An Eulerian definition of entrainment rate per unit span and from both sides of the layer is simply the rate of increase of the recirculating area of the cat's-eye (figure 15*a*). The fluid that enters this area is mostly irrotational. For an evaluation of the fraction of the fluid that is mixed as it enters the cat's-eyes in the two-dimensional flow see Corcos & Sherman (1976). For the mixing layer, entrainment by and large precedes mixing and the resulting recirculation predisposes the fluid to mixing by a mechanism whose two-dimensional version is discussed below but which is considerably enhanced by three-dimensional secondary motion.

If the fluid on the two sides of the mixing layer can be identified separately, it will appear to be drawn within the cat's-eye on either side of the rolled-up material surface initially separating the streams. Many experimental workers refer to this descriptively as 'engulfing'. Another way to look at it (figure 15*b*) is to realize that the fluid particles are solicited by the velocity field along open oscillating streamlines leading downstream when these streamlines are outside the cat's-eye boundary and by that along closed streamlines when the cat's-eye boundary has grown so as to include them.

3.6.4. *Rate of molecular mixing*

It is useful to define a measure of mixedness, the degree to which the shear layer has diffused a scalar ρ which was initially found in different concentrations in the two streams.

† In work recently completed, Kaul (1982) has evaluated the perturbation created upstream by the presence of several vortices in the process of pairing. The vorticity of the T-layer is first calculated by finite differences. The S-layer vorticity is then mapped from that in the T-layer by a Galilean transformation supplemented by additional sources (upstream and downstream) required to satisfy boundary conditions. This allows the calculation of the induced velocity in the S-layer. It is compared with the velocity at the same point which would be obtained by a direct Galilean mapping of the T-layer velocity. For frequencies corresponding to the fundamental and to the first subharmonic, and even when one stream is at rest, he finds that neither the amplitude nor the phase are altered by a considerable amount.

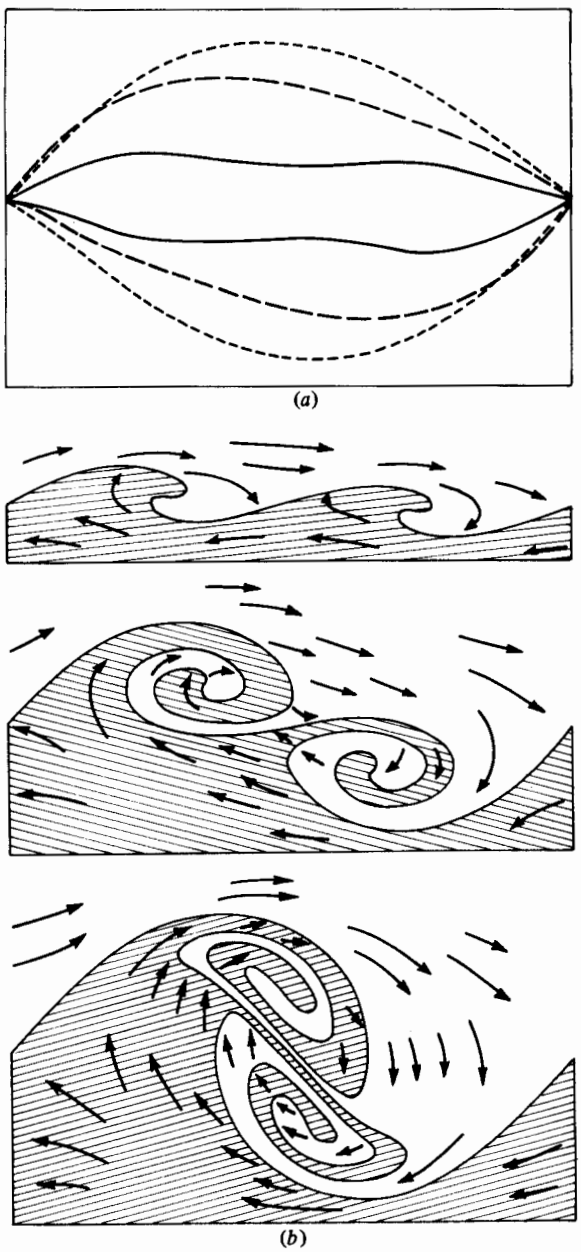

FIGURE 15. Two views of entrainment: (*a*) the rate of growth of the cat's-eye ($\tau = 1.0$; 2.0; 2.5); (*b*) the visual record of 'engulfing'. The latter appears when a scalar fluid attribute with small diffusivity is segregated by the material interface. Here the interfacial evolution is taken from figure 7. The arrows are segments of streamlines. Their lengths are arbitrary. From top to bottom: $\tau = 1.0$; 2.0; 2.5.

Let ρ have asymptotic values $-\rho_1$ far above and ρ_1 far below the shear layer. Define the mixed volume V_m (per unit span) by

$$V_m = \iint_{\rho>0} \left(1-\frac{\rho}{\rho_1}\right) \mathrm{d}A + \iint_{\rho<0} \left(1+\frac{\rho}{\rho_1}\right) \mathrm{d}A. \tag{3.6}$$

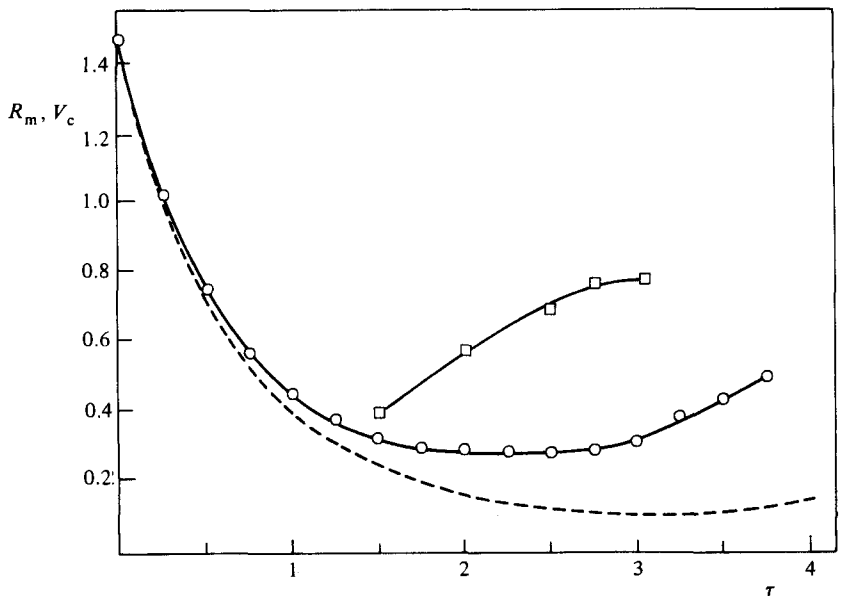

FIGURE 16. Scalar mixing in roll-up and pairing: ○, the ratio R_m of mixed volume to the cat's-eye volume (per unit span); □, cat's-eye volume V_c; ---, R_m, if mixing were due to simple diffusion. $Pr = 1$.

The integral of ρ itself over the whole plane is invariant if ρ satisfies (3.1*c*) and if there is no flux through the boundaries. But there is a flux of the quantity $E_u \equiv 1-\rho/\rho_1$ through the curve $\rho = 0$, so that

$$\frac{d}{dt}\iint_{\rho>0} E_u \, dA = D\int_{\rho=0} (\nabla E_u)\cdot \boldsymbol{n}\, ds,$$

where $\boldsymbol{n}$ is the outward normal to the contour $\rho = 0$. A similar expression holds for the quantity $E_e \equiv 1+\rho/\rho_1$ in the corresponding volume where $\rho < 0$, so that, if, at time $\tau = 0$, the concentration is ρ_1 everywhere above and $-\rho_1$ everywhere below the dividing surface,

$$V_m = -2D\int_0^t \int_{\rho=0} (\nabla E_u)\cdot \boldsymbol{n}\, ds\, dt'.$$

$\rho_1 V_m$ is the total mass of the product in a binary diffusion-limited reaction with equivalence ratio of unity if the mass fraction at ∞ of one of the reactants is ρ_1. Note that V_m equals the integration volume (i.e. its mean value) if $\rho = 0$ throughout the volume, and $V_m = 0$ if the only two possible values for ρ are the asymptotic values ρ_1 and $-\rho_1$.

The value of V_m can easily be calculated as a function of time from the numerical solution of (3.1*c*). The result is given on figure 16 for a roll-up and pairing, for $Pr = \nu/D = 1$. On these figures V_m is non-dimensionalized by the cat's-eye area V_c. If the scalar ρ had been mixed by molecular diffusion unaided by the strain associated with the vorticity concentration, the same ratio would be given by the dotted curve.

It will be noticed that, while the initial mixed volume is larger than the area V_c of the cat's-eye, the ratio $R_m = V_m/V_c$ first decreases very sharply with increasing time because initially, the strain being small, V_m increases by unaided diffusion, i.e. as $(\tau+\tau_0)^{\frac{1}{2}}$ (where τ_0 is the time required to diffuse the concentration layer from a discontinuity to the initial thickness δ_i) while V_c grows exponentially.

But, as the material interface is convuluted into several folds, the mixing rate evidently increases. In figure 16(*b*) R_m is nearly constant during a time interval for which the cat's-eye growth rate V_c is a maximum, i.e. the mixing rate keeps up with the entrainment rate.

The final rise of the value of R_m is not significant, because it occurs when the cat's-eye area stops growing for lack of further pairing. Also, in the example shown on the figure, the ratio of mixed volume to that which would have taken place at the same time by simple diffusion is not large (about three at the end of pairing). This is due primarily to the low value of the Péclet number of the flow: simple diffusion for that case would have generated a mixed volume equal to 10% of the maximum cat's-eye area (at $\tau = 2.75$).

3.6.5. *Advection in the neighbourhood of the material interface*

The picture that has emerged from our discussion of the two-dimensional shear layer is as follows: within a general outline which is the average wedge (in time or streamwise distance) of height d containing the vortices, the material interface that originally separated the two streams is distorted in a series of spiralling sheets and the vorticity is distributed in a layer on either side of this sheet whose typical thickness δ is a decreasing fraction of d. The centre of the spiralling sheet is a solid core of vorticity whose average radius r is larger than δ and smaller than d. The rest of the flow within the wedge is irrotational. For many purposes, which include the study of the development of secondary motions, diffusion of scalars, reaction and combustion between the two streams, it is often in the neighbourhood of the thin sheet (the material interface between the two streams) that the advective properties of the flow need to be known.

Now numerical solutions of the two-dimensional Navier–Stokes equations are naturally Reynolds-number dependent and do not readily lend themselves to direct generalizations and asymptotic inferences. It is thus useful to develop alternative methods. One was given by Guiraud & Zeytounian (1977, 1979). Another was applied selectively to the simplest part of the shear layer in Corcos & Sherman (1976). The same method was later used by Marble (1984) to study the effect of a single diffusive point vortex on a diffusion-controlled reaction at the initially plane boundary between two volumes of dissimilar and reacting fluids. Neu (1984*a*) was led to precisely the same approximation by a more formal asymptotic analysis of the Marble problem.

The approximation is applicable when a thin diffusive layer (of vorticity or of a passive scalar) originally centred on the material interface has been subjected to consistent extension by the strain along the interface. As a result it remains thin, and the lengthscale is much longer for gradients along the interface than across it. We are led to it as follows.

Consider for instance the transport of a scalar ρ according to

$$\rho_t + \boldsymbol{u}\cdot\boldsymbol{\nabla}\rho = D\nabla^2\rho, \tag{3.7}$$

with idealized initial conditions $\rho = 1$ in a domain $\mathscr{D}$ bounded by a curve $\mathscr{B}$ on which $\rho = 0$, where $\mathscr{B}$ is a material interface. If D is non-dimensionally very small, we expect the variation of ρ along the spiral to be slow compared to variations normal to it, which leads to the parabolic approximation

$$\rho_t + \boldsymbol{u}\cdot\boldsymbol{\nabla}\rho = D\frac{\partial^2\rho}{\partial n^2}, \tag{3.8}$$

where n is the local normal to the spiral curve. But further, if the flow consistently elongates the interface $\mathscr{B}$, by continuity there is an inflow of fluid towards this surface. With local coordinates fixed in the interface such that s is tangent to the interface, and n normal to it, and with corresponding velocity components u_s and w, we may approximate $u_s(s,n,t)$ by $u_s(s,0,t)$ and w by $-n\gamma(s,0,t)$, where $\gamma = (\partial u_s/\partial s)_{n=0}$. If we then view $u_s(s,0,t)$ and $\gamma(s,0,t)$ as Lagrangian functions of the initial location of any point on the material interface and of time τ, (5.3) becomes

$$\left[\left(\frac{\partial}{\partial\tau}\right)_{s_0} - n\gamma(s_0,\tau)\frac{\partial}{\partial n}\right]\rho = D\frac{\partial^2\rho}{\partial n^2}. \tag{3.9}$$

The strain γ need only be known along a single time-dependent curve, the material interface. In the absence of an analytical solution or model for $\gamma(s_0,\tau)$, this function is provided by calculations such as the ones discussed in §§3.3 and 3.5.3 (pp. 47–49) and illustrated on figure 2.

Illustration: the spanwise vorticity distribution. In the two-dimensional layer, the spanwise vorticity obeys

$$\frac{\partial\Omega_2}{\partial t} + u\frac{\partial\Omega_2}{\partial x} + w\frac{\partial\Omega_2}{\partial z} = \nu\left(\frac{\partial^2\Omega_2}{\partial x^2} + \frac{\partial^2\Omega_2}{\partial z^2}\right). \tag{3.10}$$

Here we neglect not only diffusion along the interfacial direction but also the effect on Ω_2 of the rotation of our local coordinate system, which can be shown to be small at high Reynolds numbers. In our local coordinates we thus rewrite (3.10) as

$$\frac{\partial\Omega_2}{\partial\tau} - n\gamma\frac{\partial\Omega_2}{\partial n} = \nu\frac{\partial^2\Omega_2}{\partial n^2}, \tag{3.11}$$

and we assume

$$\Omega_2 \to 0 \quad \text{as} \quad \frac{n}{\delta} \to \pm\infty,$$

where δ is the local vorticity thickness. A similarity solution exists for any $\gamma(s_0,\tau)$. It was given in Corcos & Sherman (1976) in the form†

$$\Omega_2(\eta,\tau) = \frac{S(\tau)}{\delta(\tau)}H(\eta), \tag{3.12}$$

where $S(\tau) = \delta\int_{-\infty}^{\infty}\Omega_2\,\mathrm{d}\eta$ is the shear across the layer, $\eta = n/d$. δ satisfies

$$\delta^2 = \delta^2(\tau_0)\exp\left[-\int_{\tau_0}^{\tau}2\gamma(\tau')\,\mathrm{d}\tau\right] + \pi\nu\int_{\tau_0}^{\tau}\exp\left[-\int_{\tau'}^{\tau}2\gamma(\tau'')\,\mathrm{d}\tau''\right]\mathrm{d}\tau', \tag{3.13}$$

while S satisfies

$$S' + \gamma S = 0, \tag{3.14}$$

in which case

$$H = \exp\left(-\tfrac{1}{4}\pi\eta^2\right). \tag{3.15}$$

Thus the vorticity distribution can be evaluated once $\delta(0)$ and $S(0)$ are specified.

We note that this simple solution will in general seriously depart from the predictions of Kelvin's vorticity theorem for an inviscid fluid. In particular, the combinations of positive strain rate γ and of viscosity (no matter how small) leads to a rapid decrease in the local value of the vorticity as well as of the shear S. For instance if the strain rate is independent of τ, $S = S_0\,\mathrm{e}^{-\gamma\tau}$, and $\delta \to (\pi\nu/2\gamma)^{\frac{1}{2}}$ in a time

† The non-homogeneous term in equation (2.10) of Corcos & Sherman (1976) is missing for our uniform-density case, so that the relevant equation for the shear is (2.15) rather than (2.18).

of order $[(\delta_i/\delta_a)^2-1]^{\frac{1}{2}}\gamma^{-1}$, where δ_i is the initial and δ_a the asymptotic value of the thickness, so that

$$\Omega_2(\tau,0)=\frac{S}{\delta}\to 0,$$

in a time of the same order. Thus for points on the sheet that are subjected to a steadily positive and large strain (such as the stagnation points), *both the total shear across the sheet and the local vorticity* within it disappear rapidly. Wherever elements of material surfaces within the vortex sheet have suffered only small positive strain or have experienced negative strain, the total shear across the vortex sheet and the local vorticity will remain high, the shear, conceivably higher than its original value, the local vorticity only slightly less.

A similar treatment can be used (Corcos & Sherman 1976; Corcos 1979) to describe the evolution of the scalar ρ, whose distribution is found to be

$$\rho=\tfrac{1}{2}\Delta\rho\,\mathrm{erf}\{(\tfrac{1}{2}D)^{\frac{1}{2}}\eta_M\},$$

where D is the molecular diffusivity, $\eta_M=n/\delta_M$, and δ_M is given by (3.13) with D substituted for γ. As remarked in §3.4.2, the magnitude of the gradient of the scalar ρ is thus inversely proportional to the diffusion thickness δ_M.

3.6.6. *The core*

Towards the centre of the coiling interfacial spiral (the core), advected and diffusive attributes that straddle neighbouring folds eventually merge, because having been stretched less, or compressed, their diffusive thickness is larger, and/or because the advective pattern in the recirculating region forces neighbouring folds of the material interface ever closer together.

Here the boundary conditions on either side of a diffusive layer clearly need to be modified, but in addition, the parabolic approximation may not be applicable. Returning to (3.7) and (3.9), we see that this approximation requires both the initial condition $\partial\rho/\partial n \gg \partial\rho/\partial s$, and locally $D/\gamma L^2 \ll 1$, where L is the scale for variations of ρ along the material interface. In particular, where γ vanishes (as it must in regions of solid-body rotation) or oscillates between positive and negative values (whenever the deformation is caused primarily by quasi-stationary distant centres of vorticity), the parabolic approximation should and does fail. A manifestation of this failure is the presence of large angles between the material interface and the local direction of constant-concentration lines (see figure 4 for instance). This departure occurs in our calculations for a relatively large central part of the spiral because we chose $Pr=1$, but it would likely occur somewhere in the core even if $Pr \gg 1$. On the other hand, in the Marble example problem, as Neu (1984*a*) shows, the parabolic approximation is uniformly valid, essentially because γ is always positive in that case and increases monotonically as the distance from the spiral centre decreases.

3.6.7. *The scales of the flow*

The previous discussion shows that one may define three characteristic lengthscales in the two-dimensional shear layer for each diffusive attribute of the flow such as spanwise vorticity or concentration. For the concentration ρ, for instance, these are as follows.

(1) The asymptotic thickness δ_M of the diffusion layer (for constant value of γ and large times):

$$\delta_M=\left(\frac{\pi D}{2\gamma}\right)^{\frac{1}{2}}.$$

This is a reasonable estimate for the minimum diffusion-layer thickness near the stagnation points where γ is always > 0 and near climax (when γ varies slowly). From our calculations around that time, $\gamma \approx 3U/\lambda$, where λ is the periodic spacing between vortices. Thus

$$\delta_{\mathrm{M}} = \lambda\left(\frac{\pi D}{6U\lambda}\right)^{\frac{1}{2}}.$$

(2) The typical total height d of the interfacial spiral that is approximately $\frac{1}{2}\lambda$ at climax. Thus the ratio of the first two characteristic scales is

$$\frac{\delta_{\mathrm{M}}}{d} \approx 2\left(\frac{D}{U\lambda}\right)^{\frac{1}{2}}.$$

(3) The third lengthscale is the radius r_{M} of that part of the scalar distribution which has evolved into a central solid core with weak gradients. This radius has not been evaluated. It is the radial distance from the spiral centre to a circle on which a diffusion-layer thickness δ_{M} is equal to the typical spacing between two neighbouring branches of the spiral. For the Marble model problem, if we identify the vortex circulation Γ with $2U\lambda$,

$$\frac{r_{\mathrm{M}}}{d} \approx \left(\frac{D}{U\lambda}\right)^{\frac{1}{6}}.$$

Similarly there are three lengthscales associated with the vorticity distribution. These are d, δ and r, where r is defined by analogy with r_{M} and where

$$\delta = \left(\frac{\pi\nu}{2\gamma}\right)^{\frac{1}{2}}.$$

Since $\delta/d \simeq (1/Re)^{\frac{1}{2}}$, δ can be viewed as the Taylor microscale for the shear layer. As argued in Corcos (1979), no purely two-dimensional secondary local shear instability is possible if the flow is barotropic, so that δ is the smallest possible lengthscale for a two-dimensional shear layer. In fact, as we saw in §3.5, δ may not be properly a thickness scale for *spanwise* vorticity layers since in the asymptotic limit for which it is defined (γ = constant, $t \to \infty$, i.e. effectively $t > \gamma^{-1}$) that component of vorticity tends to disappear from such layers: at least it may be said that in general only weak spanwise vorticity is found in layers of that thickness. But, as will be shown in Part 3, δ as defined here is a natural lengthscale for the gradient of streamwise vorticity.

This work has been supported by the U.S. Office of Naval Research under contract N.R. 062-665.

REFERENCES

ACTON, E. 1976 *J. Fluid Mech.* **76**, 561.

AMSDEN, A. A. & HARLOW, F. H. 1964 *Phys. Fluids* **7**, 327.

ASHURST, W. T. 1979 Numerical simulation of turbulent mixing layers via vortex dynamics. In *Turbulent Shear Flow I* (ed. F. Durst *et al.*), p. 402. Springer.

BATCHELOR, G. K. 1967 *An Introduction to Fluid Dynamics*. Cambridge University Press.

BATT, R. G. 1975 Some measurements on the effect of tripping the two-dimensional shear layer. *AIAA J.* **13**, 245.

BEALE, T. J. & MAJDA, A. 1981 *Math. Comp.* **37**, 243.

BEALE, T. J. & MAJDA, A. 1982 *Math. Comp.* **39**, 29.

BRACHET, M. E. & ORSZAG, S. 1982 Secondary instability of free shear layer flows. Submitted to *J. Fluid Mech.*

BRADSHAW, P. 1966 *J. Fluid Mech.* **26**, 225.

BREIDENTHAL, R. E. 1978 A chemically reacting shear layer. Thesis, Calif. Inst. Tech.

BROWAND, F. K. 1966 *J. Fluid Mech.* **26**, 281.

BROWAND, F. K. & HO, C. M. 1983 The mixing layer: an example of quasi-two-dimensional turbulence. *J. Méc. Théor. Appl.* (to appear).

BROWAND, F. K. & LATIGO, B. O. 1979 *Phys. Fluids* **22**, 1011.

BROWAND, F. K. & TROUTT, T. R. 1980 *J. Fluid Mech.* **97**, 771.

BROWAND, F. K. & WEIDMAN, D. D. 1976 *J. Fluid Mech.* **76**, 127.

BROWN, G. L. & ROSHKO, A. 1974 *J. Fluid Mech.* **64**, 775.

CANTWELL, B. J. 1981 *Ann. Rev. Fluid Mech.* **13**, 457–515.

CHORIN, A. J. 1973 *J. Fluid Mech.* **57**, 785.

CHORIN, A. J. 1978 *J. Comp. Phys.* **27**, 428.

CHORIN, A. J., HUGHES, T. J. R., MCCRACKEN, M. F. & MARSDEN, J. E. 1978 *Commun. Pure Appl. Maths* **31**, 205.

CHRISTIANSEN, J. P. 1973 *J. Comp. Phys.* **13**, 363.

CORCOS, G. M. 1979 The mixing layer: deterministic model of a turbulent flow. *Univ. Calif., Berkeley, Coll. Engng* Rep. FM-79-2.

CORCOS, G. M. 1981 The deterministic description of the coherent structure of free shear layers. In *The Role of Coherent Structures in Modelling Turbulence and Mixing* (ed. J. Jimenez). Lecture Notes in Physics, vol. 136, p. 10. Springer.

CORCOS, G. M. & LIN, S. J. 1984 *J. Fluid Mech.* **139**, 67.

CORCOS, G. M. & SHERMAN, F. S. 1976 *J. Fluid Mech.* **73**, 241.

CORRSIN, S. 1962 *Phys. Fluids* **5**, 1301.

CORRSIN, S. & KISTLER, A. L. 1954 *NACA. TN* 3133.

DEEM, G. S. 1977 The origin of cusped waves in layered fluids (unpublished).

DELCOURT, B. A. G. & BROWN, G. L. 1979 The evolution and emerging structure of a vortex sheet in an inviscid and viscous fluid modelled by a point vortex method. In *Proc. 2nd Symp. on Turbulent Shear Flows, July 1979, Imperial Coll., London*, p. 14.35.

DIMOTAKIS, P. E., MIAKE-LYE, R. C. & PAPANTONIOU, D. A. 1982 *J. Fluid Mech.* **73**, 241.

DRAZIN, P. & REID, W. 1981 *Hydrodynamic Stability*. Cambridge University Press.

FREYMUTH, P. 1966 *J. Fluid Mech.* **25**, 683.

GUIRAUD, J. P. & ZEYTOUNIAN, R. KH. 1977 *J. Fluid Mech.* **25**, 683.

GUIRAUD, J. P. & ZEYTOUNIAN, R. KH. 1979 *J. Fluid Mech.* **90**, 197.

HALD, O. H. 1979 *SIAM J. Numer. Anal.* **16**, 726.

HO, C. M. & HUANG, L. S. 1982 *J. Fluid Mech.* **119**, 443.

HUSSAIN, A. K. M. F. 1980 Coherent structures and studies of perturbed and unperturbed jets. In *The Role of Coherent Structures in Modelling Turbulence and Mixing* (ed. J. Jimenez). Lecture Notes in Physics, vol. 136, p. 252. Springer.

HUSSAIN, A. K. M. F. & CLARK, A. R. 1981 *J. Fluid Mech.* **104**, 263.

JIMENEZ, J. 1980 *J. Fluid Mech.* **96**, 447.

JIMENEZ, J., MARTINEZ-VAL, R. & HERMAN, M. A. 1981 Shear layer models and computer analysis of data. In *The Role of Coherent Structures in Modelling Turbulence and Mixing* (ed. J. Jimenez). Lecture Notes in Physics, vol. 136, p. 41. Springer.

KAUL, U. K. 1982 Do large vortices control their own growth in a mixing layer? An assessment by a boot-strap method. Ph.D. thesis, Univ. Calif., Berkeley, Mech. Engng Dept.

KELLY, R. E. 1967 *J. Fluid Mech.* **27**, 657.

KONRAD, J. H. 1977 An experimental investigation of mixing in two-dimensional turbulent shear flows with applications to diffusion-limited chemical reactions. Thesis, Calif. Inst. Tech.

KOOP, C. G. & BROWAND, F. K. 1979 *J. Fluid Mech.* **93**, 135.

LAMB, H. 1932 *Hydrodynamics*. Dover.

LATIGO, B. 1979 Large-scale structure interactions in a two-dimensional turbulent mixing layer. Ph.D. thesis, Dept. Aero-space Engng, Univ. S. Calif., Los Angeles.

LAUFER, J. & MANKOVITZ, P. 1980 *AIAA Paper* 80-8062.

LEONARD, A. 1980 Vortex methods for flow simulation. *Ames Res. Center, NASA Rep.*

LIEPMANN, H. W. & LAUFER, J. 1949 Investigation of free turbulent mixing. *NACA TN* 1257.

LIN, S. J. & CORCOS, G. M. 1984 The mixing layer: deterministic models of a turbulent flow. Part 3. The effect of plane strain on the dynamics of stretched vortices. *J. Fluid Mech.* (to be published).

MARBLE, F. E. 1983 Growth of a diffusion flame in the field of a vortex. To appear in the Luigi Crocco anniversary volume.

MOORE, D. W. 1976 *Mathematica* **23**, 35.

MOORE, D. W. & SAFFMAN, P. G. 1975 *J. Fluid Mech.* **69**, 465.

NEU, J. 1984*a* The evolution of diffusion flames convected by vortices. Submitted to *J. Fluid Mech.*

NEU, J. 1984*b* The dynamics of stretched vortices. *J. Fluid Mech.* (to be published).

OVERMAN, E. A. II & ZABUSKY, N. J. 1981 Evolution and merger of isolated vortex structures. *Univ. Pittsburgh, Tech. Rep.* ICMA 81–31.

PATNAIK, P. C., SHERMAN, F. S. & CORCOS, G. M. 1976 *J. Fluid Mech.* **73**, 215.

PELTIER, W. R., HALLÉ, J. & CLARK, T. L. 1978 *Geophys. Astrophy. Fluid Dyn.* **10**, 53.

PIERREHUMBERT, R. T. & WIDNALL, S. E. 1981 *J. Fluid Mech.* **102**, 301.

PIERREHUMBERT, R. T. & WIDNALL, S. E. 1982 *J. Fluid Mech.* **114**, 59.

PUI, N. K. & GARTSHORE, I. 1978 *J. Fluid Mech.* **91**, 111.

RILEY, J. J. & METCALFE, R. W. 1980 Direct numerical simulation of a perturbed turbulent mixing layer. *AIAA 18th Aerospace Meeting, Pasadena, CA: AIAA Reprint* 80-0274.

ROSHKO, A. 1976 Structure of turbulent shear flows: a new look. Dryden Lecture. *AIAA Reprint* 76–78.

SAFFMAN, P. G. 1968 Lectures on Homogeneous Turbulence. In *Topics on Non-Linear Physics* (ed. N. Zabusky), p. 485. Springer.

SATO, H. 1956 Experimental investigations of the transition of laminar separated layer. *J. Phys. Soc. Japan* **11**, 702.

SHERMAN, F. S. 1979 User's guide to program Khint. *Univ. Calif. Rep., Dept. Mech. Engng.*

STUART, J. T. 1967 *J. Fluid Mech.* **29**, 417.

SYNGE, J. L. & LIN, C. C. 1943 *Trans. R. Soc. Canada* **37**, 45.

TANAKA, H. 1975 *J. Met. Soc. Japan* **53**, 1.

TENNEKES, H. 1968 *Phys. Fluids* **11**, 669.

THORPE, S. A. 1971 *J. Fluid Mech.* **46**, 289.

TOWNSEND, A. A. 1951 *Proc. R. Soc. Lond.* A **208**, 534.

VAN DYKE, M. 1982 *Album of Fluid Motion.* Parabolic.

WILLE, R. 1963 Growth of velocity fluctuations leading to turbulence in a free shear layer flow. *Rep.* AFOSR-TR-AF **61** (052), p. 412.

WINANT, C. D. & BROWAND, F. K. 1974 *J. Fluid Mech.* **63**, 237.

WYGNANSKI, I. & FIEDLER, H. E. 1970 *J. Fluid Mech.* **41**, 327.

WYGNANSKI, I., OYSTER, D., FIEDLER, H. & DZIOMBA, B. 1979 *J. Fluid Mech.* **93**, 325.

ZABUSKY, N. J. 1981 *Ann. NY Acad. Sci.* **373**, 160.

ZABUSKY, N. J. & DEEM, G. G. 1971 *J. Fluid Mech.* **47**, 353.

ZABUSKY, N. J., HUGHES, M. H. & ROBERTS, K. V. 1979 *J. Comp. Phys.* **30**, 96.

ZABUSKY, N. J. & OVERMAN, E. A. 1981 Regularization of contour dynamical algorithms. *Univ. Pittsburgh Tech. Rep.* ICMA 81-22.